In every way that matters, anything the mind imagines, exists. The existence stems either from an external idea perceived by the mind, or an internal notion initiated by ones own creativity.

University of Alberta

Imperfect Channel Knowledge for Interference Avoidance

by

Saina Lajevardi

A thesis submitted to the Faculty of Graduate Studies and Research in partial fulfillment of the requirements for the degree of

Master of Science
in
Communications

Department of Electrical and Computer Engineering

University of Alberta

Faculty of Graduate Studies and Research

The undersigned certify that they have read, and recommend to the Faculty of Graduate Studies and Research for acceptance, a thesis entitled **Imperfect Channel Knowledge for Interference Avoidance** submitted by Saina Lajevardi in partial fulfillment of the requirements for the degree of **Master of Science**.

Dr. Christian Schlegel
Supervisor

Dr. Behrouz Nowrouzian
Co-Supervisor

Dr. Bruce F. Cockburn

Dr. Iannis Nikolaidis
External Examiner

Date: ____________________

To my mom, Mitra, who has always been the angel of my life.

Abstract

This thesis examines various signal processing techniques that are required for establishing efficient (near optimal) communications in multiuser multiple-input multiple-output (MIMO) environments. The central part of this thesis is dedicated to acquisition of information about the MIMO channel state - at both the receiver and the transmitter. This information is required to organize a communication set up which utilizes all the available channel resources. Realistic channel model, i.e., the spatial channel model (SCM), has been used in this study, together with modern long-term evolution (LTE) standard.

The work consists of three major themes: (a) estimation of the channel at the receiver, also known as tracking; (b) quantization of the channel information and its feedback from receiver to the transmitter (feedback quantization); and (c) reconstruction of the channel knowledge at the transmitter, and its use for data precoding during communication transmission.

Acknowledgements

It is a great pleasure for me to thank my supervisor, Dr. Christian Schlegel, for his guidance throughout this work. I am specially obliged to Dr. Dmitry Trukhachev for his endless care and patience; this thesis would have not be completed without his help. I would like to thank my amazing friends: Mahdi Ramezani for his helpful discussions on communications systems, as well as his expertise in LaTeX; Rasoul Milasi and Sahar Movaghati for their encouragement and research advice; my old friends, Obilor Nawmadi and Mahdi Rahimi, for their support from far away (through online chats and emails). I drew tremendous strength from members of my family: from my mother, father, brother, and older sister, who live so far away, and from my little sister, Parmida, and my wonderful friend and roommate, Reihaneh Rabbany, who are with me in Edmonton.

I would like to acknowledge contributions from my colleagues, Marcel Jar, Majid Ghanbarinezhad and Russel Dodd, who each in his own way had helped with the completion of this work.

Friendship for me is the strength to keep working and to follow my dreams. Here, I would like to acknowledge my great friends: Mahdi Ramezani, Dr. Mohammad Behnam, Mohammad Mehdi Khajeh, Navid Paydavousi, and Farzaneh Saba, who have always been supporting me in both good and bad times. Their unconditional friendship was something I could always count on. Finally, I would like to thank my best friend, Dr. Anthony Yeung, for his intellectual support and attention during the last stages of my work. His support and friendship encouraged me to keep up the hard work and to remain optimistic at all times.

Table of Contents

1 Introduction **1**
1.1 Motivation . . . 1
1.2 Wireless Communications with Multiple Antennas . . . 2
1.3 Mobile Cellular Communications . . . 3
1.4 Thesis Outline . . . 5

2 Background **7**
2.1 The Capacity of MIMO Channels . . . 7
2.2 Beamforming . . . 8
2.2.1 beamforming with Multiple Users . . . 9
2.2.2 Downlink Beamforming . . . 10
2.3 The Long-Term Evolution System (LTE) . . . 12
2.3.1 LTE Specifications . . . 12
2.3.2 LTE Transmission Format . . . 13
2.4 The Spatial Channel Model (SCM) . . . 15

3 Channel Estimation **19**
3.1 The Estimation Problem . . . 19
3.2 Wiener Filter . . . 20
3.2.1 Principle of Orthogonality . . . 21
3.3 Methods of Steepest Descent (SD) and LMS Algorithm . . . 23
3.3.1 The SD Algorithm . . . 24
3.3.2 Stochastic Gradient-Based Algorithms: the LMS Approach . 25
3.4 Example: Channel Estimation in the MIMO Scenario . . . 27

4 Channel State Information Feedback and Quantization **32**
4.1 Finite-Rate Feedback of CSI . . . 32
4.2 Feedback Quantization for Multiuser MIMO, Problem Definition and Approach . . . 34
4.3 Codebook Design . . . 37
4.3.1 Random Vector Quantization (RVQ) . . . 38
4.3.2 Grassmannian Line(Subspace) Packing . . . 39
4.4 Experimental Results . . . 40
4.4.1 Joint Channel Estimation and Quantization Feedback . . . 43

5 Limited Feedback in Time-Varying Multipath MIMO Channels **46**
5.1 Multipath Channel Model 47
5.1.1 LTE Multipath Characteristics 48
5.2 Channel Estimation in MIMO-OFDM 49
5.2.1 Channel Estimation in LTE 50
5.2.2 OFDM Structure in Terms of Estimation 51
5.3 LTE Channel Reconstruction at Transmitter 53
5.4 Feedback Schemes for Multipath MIMO Channels with LTE 54

6 Concluding Remarks and Future Work **58**

Bibliography **61**

List of Figures

1.1 Basic communication system for MIMO channels. 3
1.2 Illustration of the interference dominance in cellular networks. 4
1.3 Sampled target and interferer power distribution for the SCM. The interferer is at distance 550m [1] – see Figure 1.2. 5

2.1 Mathematical basics of beamforming. 9
2.2 Downlink beamforming using precoding separation among different users. 10
2.3 LTE resource block. 11
2.4 LTE frame structure. 13
2.5 BS and MS angular parameters [1]. 15

3.1 Filtering system block diagram. 20
3.2 Uplink transmission scenario. Two vehicles are approaching one another, each at a speed of 60km/h. 27
3.3 LMS channel tracking for the reference transmitter. 28
3.4 Autocorrelation function of the residual error of the LMS channel estimation. 29
3.5 Projection loss for two passing transmitters. 30
3.6 Projection loss for two passing transmitters where the LMS is used to estimate the interfering channel with samples taken every 1ms. . . 31

4.1 Capacity performance of Grassmannian and Random Vector Quantization with 2 and 3 feedback-bit. 39
4.2 Capacity performance of Grassmannian and Random Vector Quantization with a large number of bits. 40
4.3 Capacity performance of Grassmannian and Random Vector Quantization with a constant number of feedback bits. 41
4.4 LMS channel tracking of the power of the wireless channel from the first BS antenna to the MS. 42
4.5 Autocorrelation function of the residual error. 43
4.6 Capacity performance using different forms of CSIR and CSIT. . . . 44

5.1 ISI in OFDM system. 47
5.2 Multipath delay spread histogram in the macro urban scenario. . . . 49
5.3 Frequency response of the multipath in macro urban scenario-HSDP. 50
5.4 Frequency response of the multipath in macro urban scenario-LTE. . 51
5.5 LTE time-frequency resource grid with pilot locations. 52

5.6 SCM signal Reconstruction with Doppler rate and 8-bit feedback per sample. 53
5.7 SCM signal Reconstruction sampled at 4 times Doppler rate with 2 bits of feedback per sample. 54
5.8 ZF capacity performance for LTE. 57

List of Tables

2.1 Transmission bandwidth configuration for LTE. 12
2.2 Channel quality indicator table. 14
2.3 Sub-path angle offsets for AoD and AoA. 16

4.1 Grassmannian generated codebook for $M = 3$ and $N = 2^3 = 8$. 37

5.1 SCM signal reconstruction comparison at the transmitter. 55

List of Symbols

Symbol	Definition	First Use
$\mathbf{A}_{m\times n}$	An m by n matrix	2
η	Gaussian noise	2
$\mathbf{a}$	A vector	3
τ	Time delay	3
P_t	The transmit power	7
C	The channel capacity	7
ρ	The signal-to-noise ratio	7
$\mathbf{H}$	The channel matrix	7
$\mathbf{Q}$	The covariance matrix	7
$\mathrm{tr}(\cdot)$	Trace of the enclosed matrix	7
$\det(.)$	Determinant of the enclosed matrix	7
$\mathbf{I}$	The identity matrix	7
N	Number of receive antennas	7
$\mathbb{E}$	Expected value operator	8
$(.)$	The complex conjugate	8
$\lvert.\rvert$	The vector Euclidean norm	8
$(.)^{-1}$	The matrix inverse	9
$\mathcal{P}$	The projection vector	9
J	Cost function for formulating Wiener filtering problem	21
$(.)^H$	The conjugate transpose (Hermitian)	24
$\mathbf{p}$	Cross-correlation vector	24
$\mathbf{R}$	Ensemble-average correlation matrix	24

∇	Gradient vector	25
δ	Regularization parameter	26
μ	Step-size parameter in steepest-descent or LMS algorithm	26
$\mathbf{P}$	The pilot signal	27
M	Number of transmit antennas	33
$(.)^{\dagger}$	The matrix pseudo-inverse	35

List of Abbreviations

Abbrv.	Definition	First Use
MIMO	Multiple-input multiple-output	1
OFDM	Orthogonal frequency-division multiplexing	1
LTE	Long-term evolution	1
CDMA	Code division multiple access	1
CSIR	Receiver channel state information	1
CSIT	Transmitter channel state information	2
ZF	Zero-forcing	2
i.i.d.	Independent and identically distributed	3
SISO	Single-input single-output	3
BS	Base station	3
MS	Mobile station	3
SCM	Spatial channel model	4
SNR	Signal-to-noise ratio	7
MRC	Maximum ratio combining	8
TDD	Time-division duplexing	11
SC-FDMA	Single-carrier frequency-division multiple-access	12
PAPR	Peak-to-average power ratio	13
LOS	Line-of-sight	16
AoD	Angle of departure	16
AoA	Angle of arrival	16
RLS	Recursive least squares	20
SD	Steepest descent	20

LMS	Least mean squares	20
MMSE	Minimum mean square estimation	21
SGBA	Stochastic gradient-based algorithms	25
WSS	Wide-sense stationary	25
CSI	Channel state information	32
SINR	Signal-to-interference and noise ratio	32
MU-MIMO	Multiuser MIMO	33
CQI	Channel quality information	34
CDI	Channel direction information	34
RVQ	Random vector quantization	38
ISI	Inter-symbol interference	46
NLOS	Non-line-of-sight	47
WSSUS	Wide-sense stationary uniform scattering	48
HSDPA	High-speed downlink packet access	48

Chapter 1

Introduction

1.1 Motivation

The enormous demands for high data rate and quality of service mobile communication systems are the basis for the deployment of new technologies for future of wireless communications. Multiple-input multiple-output (MIMO) and orthogonal frequency-division multiplexing (OFDM) are two such techniques which are suitable for upcoming cellular networks requirements. MIMO and OFDM are utilized as the underlying technologies for standards such as IEEE 802.11n, WiMAX, and 3GPP long-term evolution (LTE).

The emerging needs for increasingly higher data rate telecommunication introduce many new challenges into the transmission systems. LTE is the most recent standard introduced by the International Telecommunications Union (ITU) which satisfies the anticipated users' requirements, with a large number of new technological and architectural features, including OFDM as the air interface instead of wideband Code division multiple access (CDMA) as in third generation mobile (3G) systems. However, LTE is not yet a 4G technology as it does not accomplish all the requirements set forth for 4G [2]. For this reason, it has sometimes been referred to as the 3.99G of cellular networks.

Some of the specifications of LTE make it a pioneer in capacity improvement and interference mitigation, which is the main motivation of this thesis. Larger network coverage, higher quality services and faster transmission rates all lead to interference throughout the network. A thorough knowledge of the channel is critical to avoiding interference by the different transmission techniques. The acquisition of channel state information at the receiver (CSIR) is done by adaptive channel estimation techniques. Providing the transmitter with this knowledge will bring up another set of challenges to the system which is typically addressed by feedback. Utilizing the channel information at the transmitter (CSIT), the transmitter applies precoding techniques to reduce interference over the entire system. This will be discussed further throughout this thesis. In this thesis, the zero-forcing (ZF) capacity with perfect channel knowledge is determined as the system's upper bound on achievable performance. Also, we limit the multiuser MIMO system to either two users or single-antenna mobile terminals.

1.2 Wireless Communications with Multiple Antennas

MIMO is a key technology to enabling high data rate transmission in wireless communications; see Section 1.1. High data rate transmissions on the order of a giga-byte seems feasible with MIMO transmission technology [3]. One can regard MIMO as an extension of smart antenna [4]. The objective of a smart antenna is to concentrate all the transmitted energy to the point of interest. In essence, MIMO transmits data in all channel matrix dimensions with no additional power and bandwidth. Thus, the benefits of MIMO go beyond the smart antenna concept.

MIMO has been the main vehicle in mobile wireless communications for several years now. The studies of Alamouti and Tarokh introduced a new dimension to the field of MIMO known as space-time coding [5, 6]. According to [7], MIMO studies can be classified into three main fields: information and coding theory, channel modeling and adaptive signal processing, and antenna arrays.

Priliminary Concepts

The composite MIMO channel with a matrix $\mathbf{H}_{N\times M}(\tau, t)$ consists of N receive antennas and M transmit antennas; see Fig. 1.1. The discrete-time input-output relation for signal transmission over a single carrier is given by

$$\mathbf{y} = \sqrt{\frac{E_c}{M}}\mathbf{Hc} + \eta$$

where $\mathbf{c}$ is the transmitted signal, and E_c is the total transmitted power.

The received signal $y_j(t)$ at the jth antenna is given by

$$y_j(t) = \sum_{i=1}^{M} h_{ji}(\tau, t)c_i(t) + \eta_j(t), \tag{1.1}$$

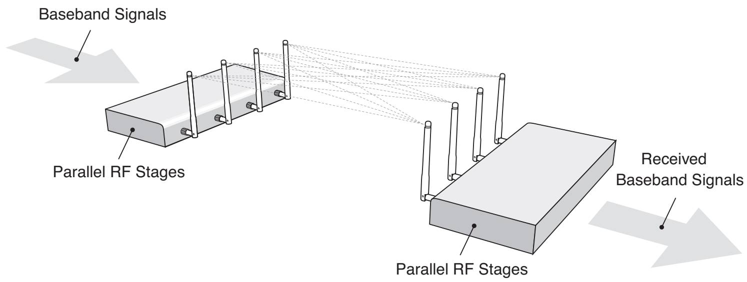

Figure 1.1: Basic communication system for MIMO channels.

where $\eta_j(t)$ is Gaussian receiver noise, and the path strength $h_{ji}(\tau, t)$ describes the time variation and frequency selectivity of the channel from the ith transmit antenna to the jth receive antenna.

MIMO results in an additional dimension which is known as the spatial dimension. The exact architecture for spatial multiplexing is given in [8, 9]. Spatial multiplexing gain improves the spectral efficiency of the channel with no requirement for additional power and bandwidth, where different data streams are transmitted over different antennas and received independently. From an information theoretic point of view, the amount of information that a transmission system is capable of carrying is given by the Shannon capacity [10], which is further discussed in the following section.

The original papers on MIMO capacity model the channel matrix elements ideally as independent and identically distributed (i.i.d.) Gaussian random variables which correspond to a very rich scattering environment. Different measurements of real MIMO environments have been performed in [11–13], for example. The measurements confirm the capacity improvement of MIMO compared to the traditional single-input single-output (SISO) system in urban and suburban environments. The indoor environment, however, benefits from rich multipath scattering which leads to higher spectral efficiencies.

1.3 Mobile Cellular Communications

Every cellular networks consists of a number of cells being virtually partitioned, including a base station (BS) transceiver and number of users, known as mobile stations (MS). The concept behind the partitioning is to reuse the frequency resources to serve an unlimited number of users; see Fig. 1.2. There are, however, several transmission issues in the cellular networks:

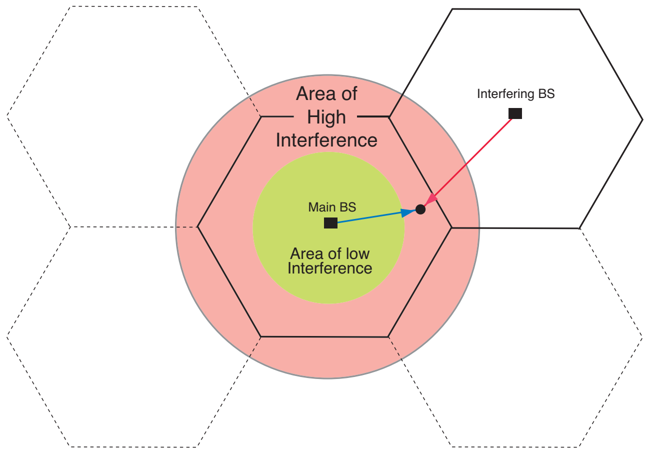

Figure 1.2: Illustration of the interference dominance in cellular networks.

1. The variety of radio transmission channels resulting from large user coverage and the shape of the cellular networks. This diversity originates from a number of reasons – such as mobility of the MS's, multipath effects, different channel paths, and random signal phase arrivals which introduce position-dependant fading to the phase and location of the radio signals.

2. The presence of interference in two forms: inter-cell interference and intra-cell interference. Intra-cell interference is technically avoided in LTE system due to channel orthogonalization. In contrast, inter-cell interference, which is interference at the cell edges, is much harder to avoid. A number of solutions, such as *cell interference coordinations*, have been proposed for LTE systems. These solutions, however, are still far from being implemented [14].

Cellular Systems: Interference

In practice, most cellular networks are interference-limited [15]. In cellular networks, a large number of MSs are subjected to strong levels of interference; see Fig. 1.2. Assuming the distribution of the users is normal, the majority of them will be close to edges and using possibly the same resources. In the analytical approach, user interference is typically regarded as white Gaussian noise for the sake of simplicity.

Fig. 1.3 shows the signal strength of a target user (purple) in comparison to the signal of an interference from a neighboring cell (green). The target MS is at 450m from the central BS, and 550m from the BS in the neighboring cell. The spatial channel model (SCM) was used to generate these samples; see Section 2.4. Even

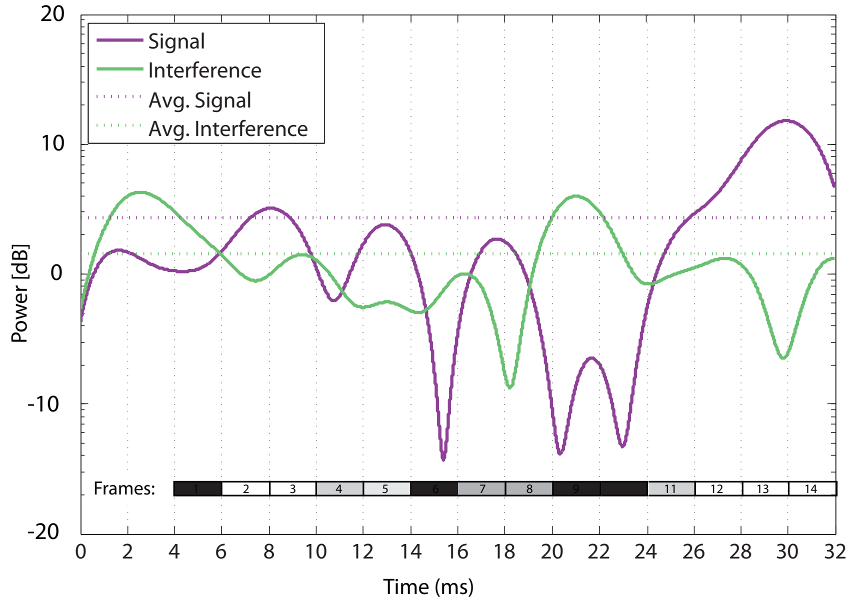

Figure 1.3: Sampled target and interferer power distribution for the SCM. The interferer is at distance 550m [1] – see Figure 1.2.

though the average received power is greater by 4dB, there is a high probability that the interference level is actually higher than the level of the target signal. Controlling this type of scenario is critical to providing high date rate transmission to cell-edge users. This issue, which will be further discussed, forms the core study of this thesis. Note that in this thesis, coordination is not considered on either downlink or uplink transmission.

1.4 Thesis Outline

Chapter 2 reviews the background and preliminaries for the whole thesis. Chapter 3 discusses adaptive channel estimation algorithms and their application to the estimation of wireless channels. Some important principles in adaptive signal processing theory are studied, and the LMS algorithm is introduced as the main channel estimator of this thesis. At the end of this chapter, simulations are performed for an uplink scenario to verify the reliability of the LMS channel estimator in a mobile environment.

Chapter 4 deals with the performance of ZF multiuser MIMO with quantized limited feedback channel knowledge at the BS. Due to multiuser transmission techniques in cellular networks, the system is subject to interference and degraded performance. The effect of quantized channel information on interference avoidance forms the core of this chapter. At the end of this chapter, the ZF performance is evaluated in the context of estimation and feedback errors. Chapter 5 is devoted to the similar concepts of interference avoidance, data precoding and limited feedback, but applied here to a more challenging transmission environment. Multipath in LTE is the channel environment of interest, and the effects of feedback of both frequency and time domain information are analyzed. Chapter 6 summarizes the key points of this thesis and addresses some possible future directions.

Chapter 2

Background

2.1 The Capacity of MIMO Channels

The amount of information which can be transmitted reliably over a channel with negligible probability of error is measured by the channel capacity. The channel capacity is basically defined by the mutual information between the input and the output signal [10]. However, proper transmission schemes are required to attain the maximum channel capacity.

Channel Capacity for Single-User System

The channel capacity of a SISO system with a transmit power constraint P_t and constant channel is given by

$$C = \log(1+\rho) \quad \text{bits/sec/Hz},$$

where ρ is the signal-to-noise ratio (SNR) of the receiver.

In practice, the channel gains change due to the multipath environment and the fading effects of wireless communications. Therefore, the ergodic (mean) capacity or average mutual information is [16]

$$C = \mathbb{E}_{\mathbf{H}}\left\{\log_2\left(1+\rho\|\mathbf{H}\|^2\right)\right\}$$

Channel Capacity for the System with Multiple Antennas

The capacity for a constant channel that is known at both end of the multiple antenna system is given by

$$C = \max_{\mathbf{Q}:\mathrm{tr}(\mathbf{Q})=P_t} \log\left[\det\left(\mathbf{I}_N + \mathbf{H}\mathbf{Q}\mathbf{H}^\dagger\right)\right]$$

where $\mathbf{Q}$ is the input covariance matrix [17].

Similarly, the ergodic capacity of the MIMO system with a flat fading channel, Gaussian noise distribution and perfect CSIT and CSIR is given by

$$C = \mathbb{E}_{\mathbf{H}} \left\{ \max_{\mathbf{Q}:\mathrm{tr}(\mathbf{Q})=P_t} \log \left[\det \left(\mathbf{I}_N + \mathbf{H}\mathbf{Q}\mathbf{H}^\dagger \right) \right] \right\}.$$

This capacity is maximized by optimizing the transmit power covariance matrix [16,17]. This occurs when P_t is distributed equally among all transmit antennas,i.e. when the covariance matrix is identity:

$$C = \max_{\mathbf{Q}:\mathrm{tr}(\mathbf{Q})=P_t} C(Q)$$

where

$$C(Q) \cong \mathbb{E}_{\mathbf{H}} \left\{ \log \left[\det \left(\mathbf{I}_N + \mathbf{H}\mathbf{Q}\mathbf{H}^\dagger \right) \right] \right\}$$

Therefore, when the covariance matrix $\mathbf{Q}$ is optimized, the ergodic capacity is

$$C = \mathbb{E}_{\mathbf{H}} \left\{ \log \left[\det \left(\mathbf{I}_N + \frac{P_t}{M} \mathbf{H}\mathbf{H}^\dagger \right) \right] \right\}$$

The expectation is taken over the distribution of the random channel matrix $\mathbf{H}$.

2.2 Beamforming

Beamforming is widely used in wireless communications, radar, sonar, speech, and biomedicine. Adaptive beamforming is used to detect the signal-of-interest at the output of antenna arrays by means of spatial filtering. Fig. 2.1 shows the basics of beamforming to a target MS. The complex vector $\mathbf{y} = \mathbf{h}c$, where

$$\mathbf{h} = [h_1, \ldots, h_N]$$

is received by all N received antennas.

To detect the signal, the receiver then applies maximum ratio combining (MRC) on the received vector $\mathbf{y}$,

$$\begin{aligned} r &= \mathbf{h}^* \mathbf{y} \\ &= \sum_{m=1}^{M} |h_m|^2 c + \eta \end{aligned} \tag{2.1}$$

The detection process of signal-of-interest can be yet extended to nulling the unwanted signals. By forcing the inner product of the received signal and the processed

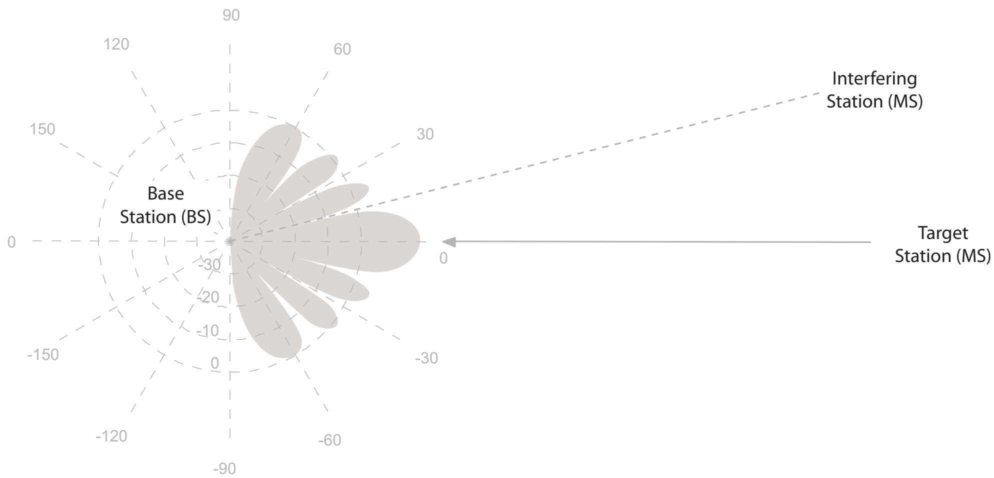

Figure 2.1: Mathematical basics of beamforming.

response vector to be zero; see Fig. 2.1, i.e.,

$$\begin{aligned} r &= \mathbf{r}^*\mathbf{y} \\ &= \eta; \quad \text{if } \mathbf{r}^*\mathbf{h} = 0. \end{aligned}$$

$\mathbf{r}$ is a projection vector to the nullspace of $\mathbf{h}$. In general, the nulling and projection process is given by

$$\mathbf{y}_{\mathrm{PR}} = \underbrace{\left(\mathbf{I} - (\mathbf{h}^*\mathbf{h})^{-1}\,\mathbf{h}\mathbf{h}^*\right)}_{\text{nulling}}\mathbf{y} = \mathcal{P}\mathbf{y}$$

In essence, all beamforming techniques deploy MRC and nulling in one form or another. In MIMO, utilization of beamforming enhances the capacity performance of the system to a large extent.

2.2.1 beamforming with Multiple Users

beamforming is a linear technique which can be applied in a variety of transmission schemes, e.g. MIMO and multiuser transmission. The linearity of beamforming allows superposition and advanced linear techniques to be applied to the beamforming process. As precoding implies, we first null the interference via $\mathbf{y}_{\mathrm{PR}} = \mathcal{P}_h\mathbf{y}$, and we then apply MRC to the projected signal. i.e.,

$$\begin{aligned} r &= {\mathbf{h}_2}^*\mathcal{P}_h\mathbf{y} \\ &= \left|\mathcal{P}_h\mathbf{h}_2\right|^2 c + \eta. \end{aligned}$$

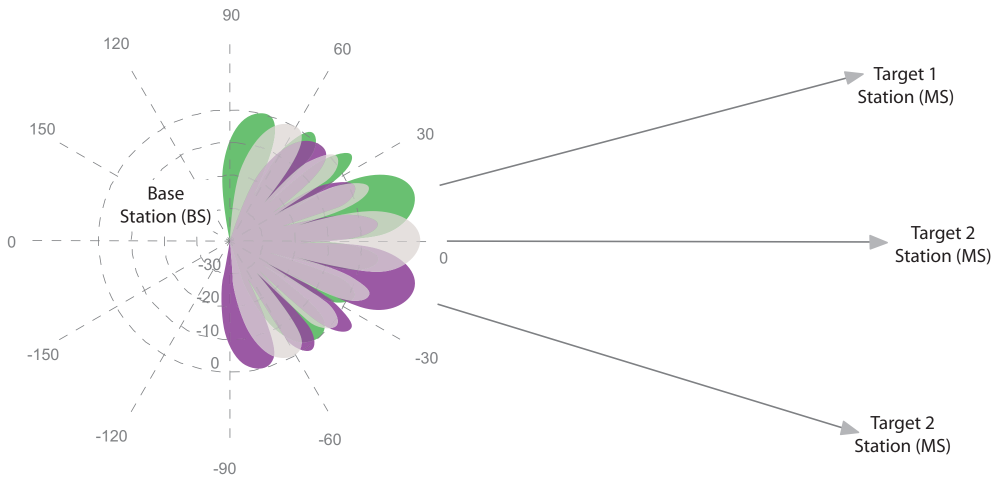

Figure 2.2: Downlink beamforming using precoding separation among different users.

$\mathbf{h}_2$ is assumed to be the signal-of-interest. Fig. 2.1 illustrates the MRC in the presence of interference.

More generally, when there are K users which access the same multi-antenna receiver, the received signal is written in the linear algebraic form essentially identical to that of a MIMO channel as

$$\mathbf{y} = \mathbf{Hc} + \mathbf{n},$$

where $\mathbf{H} = [\mathbf{h}_1, \ldots, \mathbf{h}_K]$ contains the different array response vectors as columns. The matrix pseudo-inverse

$$\overline{\mathbf{H}} = \left(\mathbf{H}^*\mathbf{H}\right)^{-1}\mathbf{H}^*$$

will simultaneously separate all the users and suppress mutual interference in a multi-beam steering process. The result is

$$\hat{\mathbf{c}} = \overline{\mathbf{H}}\mathbf{y} = \mathbf{c} + \eta. \tag{2.2}$$

The beam-former in (2.2) is also known as *ZF beam-former*. A slight variation to (2.2) is the *minimum mean-square-error* (MMSE) beam-former

$$\overline{\mathbf{H}} = \left(\mathbf{H}^*\mathbf{H} + \sigma^2\mathbf{I}\right)^{-1}\mathbf{H}^*.$$

2.2.2 Downlink Beamforming

As explained before, MIMO exploits the high data rate and spectral efficiency of the channel. beamforming techniques however, concentrate on a smaller number of paths and seek higher SNR. In the previous section, receiver beamforming was discussed

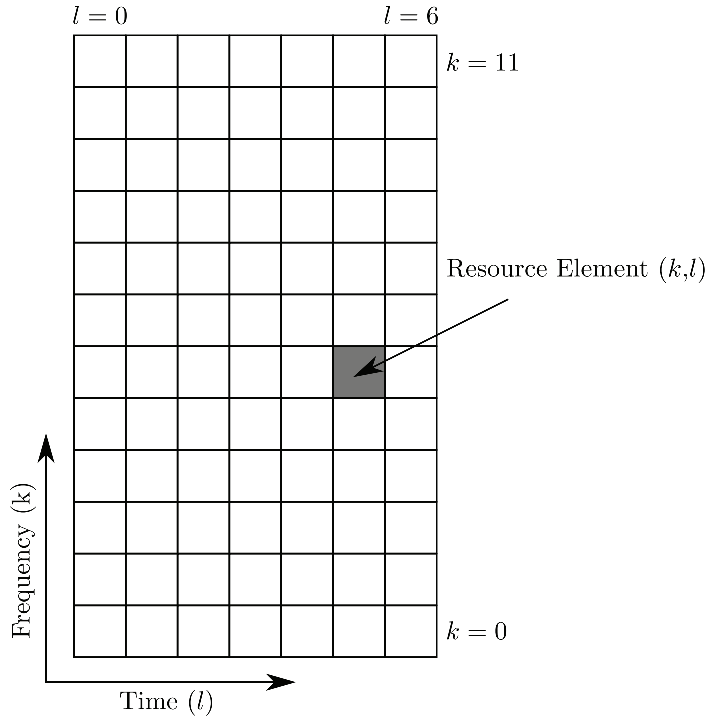

Figure 2.3: LTE resource block.

and analyzed for the detection of signal-of-interest. This process is also applicable to the transmitter subject to having identical $\mathbf{h}_k$ as the uplink; see Fig. 2.2. This is in fact the case for time-division duplexing (TDD) due to the law of reciprocity. For downlink beamforming, the arrangement needs to be somewhat modified. If we utilized a linear precoder given by the right pseudo-inverse of $\mathbf{H}$, i.e., $\hat{\mathbf{H}} = \mathbf{H}^* \left(\mathbf{H}\mathbf{H}^*\right)^{-1}$, the signals seen at the K terminals are

$$\begin{aligned} \hat{\mathbf{y}} &= \mathbf{H}\hat{\mathbf{H}}\mathbf{c} + \eta \\ &= \mathbf{c} + \eta, \end{aligned}$$

that is, mutual interference has been eliminated. Note that we cannot use an MMSE beam-former in the same straightforward way unless the noise variances at the terminals are known.

The beam-former using the right pseudo-inverse of $\mathbf{H}$ is known as a ZF transmit beam-former. The transmit precoding matrix $\hat{\mathbf{H}}$ causes the transmit powers to increase to

$$P_t = \operatorname{tr}\left(\hat{\mathbf{H}}\hat{\mathbf{H}}^*\right) = \operatorname{tr}\left(\left(\mathbf{H}\mathbf{H}^*\right)^{-1}\right)^{-1}.$$

Table 2.1: Transmission bandwidth configuration for LTE.

Bandwidth	1.4MHz	3MHz	5 MHz	10 MHz	15 MHz	20 MHz
$N_{\mathrm{sc}}^{\mathrm{RB}}$	12	12	12	12	12	12
$N_{\mathrm{RB}}^{\mathrm{UL}}$	6	15	25	50	75	100

2.3 The Long-Term Evolution System (LTE)

LTE is considered an evolution of 3G standards. Despite this evolution, LTE shares several similarities with its predecessors (except the radio interface). The advantages of LTE over the 3G standards include functionality enhancement, increased speeds, and improved performance. Apart from the high data rate transmission, which LTE enables for anticipated wireless communications, the mobility and high throughput is supported in the cell radiuses of up to 5km. LTE utilizes a number of recent technologies, such as MIMO and OFDM, to the downlink and single-carrier frequency-division multiple access (SC-FDMA) in the uplink. In the following section, some of the advantages of these methods are briefly discussed.

2.3.1 LTE Specifications

MIMO: The configuration of multiple antennas in LTE at both the transmitter and receiver is standardized in the 4G cellular networks. LTE is an advanced 3GPP project which assures downlink data rates of up to 300Mbps and increased channel capacity. LTE's physical layer is equipped with advanced technologies; such as MIMO and OFDM, which enables high data rate transmission.

Different antenna arrays are employed in an LTE system. For example, 2×2, 2×4, 4×2, or 4×4 antenna arrays is used in LTE. MIMO is an effective transmission system in terms of capacity achievement and bandwidth restrictions. Adding an antenna on either side of the communication link increases communication dimensionality and the spatial dimension; see Section 1.2. In general, a greater spatial dimension offers higher transmission data rate and capacity improvements within the available bandwidth, which saves the overall transmit power [4].

OFDM: Orthogonal frequency division multiplexing has been in use for many years. However, it has never been standardized in any cellular systems until 4G LTE. OFDM is initially a good solution to the multipath effects, in addition to being able to partition and share the frequency resources with the number of users. OFDM is used in the LTE downlink.

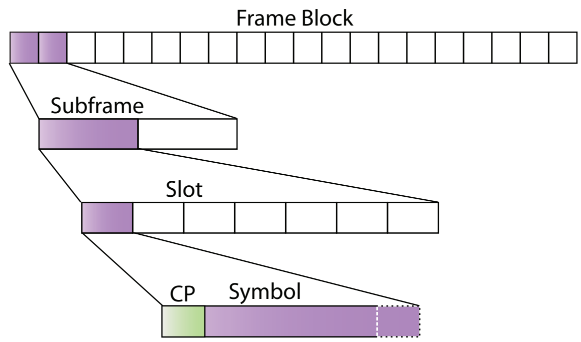

Figure 2.4: LTE frame structure.

SC-FDMA OFDM in the LTE uplink is not as effective as downlink transmission. The relativily hight peak-to-average power ratio (PAPR) is one of the major drawbacks of OFDM; it is also troublesome for uplink transmission since the user equipment (UE) is a battery-powered device. Single-Carrier FDMA, however, is an effective technique to the power constraint condition.

2.3.2 LTE Transmission Format

Fig. 2.3 (assuming a normal cyclic prefix) depicts an LTE resource block. It is the smallest form of transmission in LTE and contains two dimensions: time and frequency. Each resource block consists of 12 subcarriers with 15KHz bandwidth each. Essentially, each resource block's bandwidth is 180kHz and, depending on whether it is an uplink or downlink transmission, a different number of SC-FDMA or OFDM symbols are located in each resource block respectively [18]. Normally, 6 to 7 SC-FDMA symbols are located in each subcarrier for uplink transmission. LTE transmission configuration is listed in Table 2.1.

In addition to information symbols, one cyclic prefix is also placed in each subcarrier corresponding to OFDM symbol configuration. Each resource block transmission interval is 0.5ms. Therefore, the SC-FDMA symbol transmission time is approximately 0.5/7ms = 71.42μs. In the LTE uplink, the transmission rate is higher than that for the downlink, $12 \times 71.42\mu s = 5.95\mu$s as all 12 subcarriers are transmitted over a single carrier. The frame structure in LTE is illustrated in Fig. 2.4. Every frame consists of 20 slots and it takes 10ms for each frame to be transmitted. Every two consecutive slots is referred to as one subframe [19].

Table 2.2: Channel quality indicator table.

CQI	Modulation	Coding Rate	Bits per Resource Element
1	QPSK	0.0762	0.1523
2	QPSK	0.1172	0.2344
3	QPSK	0.1885	0.3770
4	QPSK	0.3008	0.6016
5	QPSK	0.4385	0.8770
6	QPSK	0.5879	1.1758
7	16QAM	0.3691	1.4766
8	16QAM	0.4785	1.9141
9	16QAM	0.6016	2.4063
10	64QAM	0.4551	2.7305
11	64QAM	0.5537	3.3223
12	64QAM	0.6504	3.9023
13	64QAM	0.7539	4.5234
14	64QAM	0.8525	5.1152
15	64QAM	0.9258	0.1523

Channel Quality Indicator Reporting (CQI)

CQI in LTE is the channel quality indicator which frequently reports the channel condition from the receiver to the transmitter. Table 2.2 shows the corresponding CQI with the modulation, coding rate and number of bits per resource element. The number of bits per block is given by the coding rate multiplied by the modulation order. CQI can be done in different forms of:

Wideband Feedback If the number of resource blocks is too high, feeding back the CQI indices of every block results in system overload. One can instead average the CQI over all transmission bandwidth and send the result back.

Best-M Average The average CQI of the best M channels is sent back to the transmitter.

Sub-band Feedback CQI indices corresponding to all resource blocks are transmitted from the receiver to the transmitter. The frequency of feeding back the CQI is the key factor to ensuring accurate channel state information at the transmitter side. However, if the channel does not change rapidly, CQI reporting generates unnecessary traffic overhead.

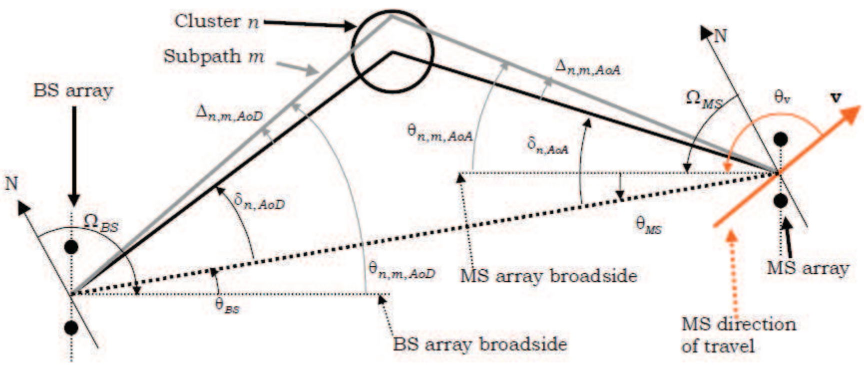

Figure 2.5: BS and MS angular parameters [1].

2.4 The Spatial Channel Model (SCM)

The spatial channel model for MIMO communication systems is represented in a technical report in the 3GPP$^{\text{TM}}$ [1]. This model was adopted by the *Wireless World Initiative New Radio* (WINNER[1]) consortium of telecommunication companies to investigate propagation conditions and develop new methods for efficient and flexible spectrum use. This model is used throughout this thesis whenever real-world channels are examined. This model generates channels with a maximum of five dimensions. Every complex channel coefficient $\mathbf{H}_n(t)$ is the channel representation of each path between one transmitter and one receiver antenna with its own delay τ_n. The dimensions are the size of receive antennas, the size of transmit antennas, the number of multipaths, the number of time samples and the number of users.

The channel model is basically a random ray-tracing model as illustrated in Fig. 2.5. Each element of $\mathbf{H}_n(t)$ is obtained by the expression

$$\begin{aligned} h_{u,s,n}(t) = \sqrt{\frac{P_L P_n \sigma_{\text{SF}}}{M}} \sum_{m=1}^{M} & \sqrt{G_{\text{BS}}\left(\theta_{n,m}^{\text{AoD}}\right)} e^{j\left(\frac{2\pi}{\lambda} d_s \sin\left(\theta_{n,m}^{\text{AoD}}\right) + \Phi_{n,m}\right)} \times \\ & \sqrt{G_{\text{MS}}\left(\theta_{n,m}^{\text{AoA}}\right)} e^{j\left(\frac{2\pi}{\lambda} d_u \sin\left(\theta_{n,m}^{\text{AoA}}\right)\right)} \times e^{j\left(\frac{2\pi}{\lambda} \|\mathbf{v}\| \cos\left(\theta_{n,m}^{\text{AoA}} - \theta_v\right) t\right)} \end{aligned} . \tag{2.3}$$

where

P_L is the path-loss which is based on the modified COST 231 Hata-Urban propagation model for urban and suburban macrocells and on the COST 231 Walfish-Ikegami non-line-of-sight (NLOS) model for microcells [20].

P_n is the normalized power of the nth path for a given pair of antennas.

[1] http://www.ist-winner.org

Table 2.3: Sub-path angle offsets for AoD and AoA.

Subpath	Offset AoD (Macrocell)	Offset AoD (Microcell)	Offset AoA
1	$+0.0894°$	$+0.2236°$	$+1.5649°$
2	$-0.0894°$	$-0.2236°$	$-1.5649°$
3	$+0.2826°$	$+0.7064°$	$+4.9447°$
4	$-0.2826°$	$-0.7064°$	$-4.9447°$
5	$+0.4984°$	$+1.2461°$	$+8.7224°$
6	$-0.4984°$	$-1.2461°$	$-8.7224°$
7	$+0.7431°$	$+1.8578°$	$+13.0045°$
8	$-0.7431°$	$-1.8578°$	$-13.0045°$
9	$+1.0257°$	$+2.5642°$	$+17.9492°$
10	$-1.0257°$	$-2.5642°$	$-17.9492°$
11	$+1.3594°$	$+3.3986°$	$+23.7899°$
12	$-1.3594°$	$-3.3986°$	$-23.7899°$
13	$+1.7688°$	$+4.4220°$	$+30.9538°$
14	$-1.7688°$	$-4.4220°$	$-30.9538°$
15	$+2.2961°$	$+5.7403°$	$+40.1824°$
16	$-2.2961°$	$-5.7403°$	$-40.1824°$
17	$+3.0389°$	$+7.5974°$	$+53.1816°$
18	$-3.0389°$	$-7.5974°$	$-53.1816°$
19	$+4.3101°$	$+10.7753°$	$+75.4274°$
20	$-4.3101°$	$-10.7753°$	$-75.4274°$

σ_{SF} represents the lognormal shadowfading coefficient. It is 8dB for macrocells, 4dB for line-of-sight (LOS) microcells and 10dB for NLOS microcells.

M The SCM approximates each one of the N resolvable paths as a sum of 20 unresolvable subpaths. $M = 20$ is fixed in this model.

$\theta_{n,m}^{\mathrm{AoD}}$ is the angle of departure (AoD). Each one of the 20 unresolvable subpaths for each one of the N resolvable paths leaves the BS with a certain departure angle; see Fig. 2.5. These angles are obtained by first obtaining the angle for the n^{th} path and then applying the offsets listed in Table 2.3 for each subpath.

$\theta_{n,m}^{\mathrm{AoA}}$ is the angle of arrival (AoA) For each resolvable path, each one of the 20 unresolvable subpaths arrives at the MS with a certain angle; see Fig. 2.5. As in the case of departure angles, these angles are obtained by first obtaining the angle for the n^{th} path and then applying the offsets listed in Table 2.3 for each subpath. The angles for the N resolvable paths are taken from the following distribution

$$\rho_n \sim \eta(0, \sigma_{n,\mathrm{AoA}}^2) \quad \text{for urban and suburban macrocells and urban microcells,}$$

where

$$\sigma_{n,\mathrm{AoA}} = 104.12\left(1 - e^{-0.2175|10\log(P_n)|}\right)$$

and

$$\sigma_{n,\mathrm{AoA}} = 104.12\left(1 - e^{-0.265|10\log(P_n)|}\right)$$

for macrocells and microcells, respectively. These angles are associated with randomly chosen resolvable paths.

$G_{\mathrm{BS}}\left(\theta_{n,m}^{\mathrm{AoD}}\right)$ is BS antenna gain. Since the BS antennas are sectorized, its gain depends on the departure angle, as seen in Section 4.5.1 of [1].

$\left(G_{\mathrm{MS}}\theta_{n,m}^{\mathrm{AoA}}\right)$ is mobile antenna gain at MS which is assumed to have an omni-directional pattern with a gain of -1dB.

λ represents the carrier wavelength in meters.

d_s is the distance of the sth antenna from the reference antenna at the BS; given in meters.

d_u is the distance of the uth antenna from the reference antenna at the MS; given in meters.

$\Phi_{n,m}$ is the phase of the mth subpath of the m^{th} path. Subpaths are (i.i.d.) with a uniform distribution in the interval $[0, 2\pi]$.

$\|\mathbf{v}\|$ is the magnitude of the MS velocity vector.

θ_v represents the angle of the MS velocity vector with respect to the MS broadside; see Fig. 2.5.

The random delays for each one of the n multipaths are obtained by first generating the following random variables:

$$\tau_n' = \begin{cases} -r_{\mathrm{DS}}\sigma_{\mathrm{DS}}\ln(z_n), & \text{for urban and suburban macrocells;} \\ z_n', & \text{for urban microcells;} \end{cases}$$

where z_n is a random variable with uniform distribution $U(0,1)$, $r_{\mathrm{DS}} = 1.4\mu$s for suburban macrocells, $r_{\mathrm{DS}} = 1.7\mu$s for urban macrocells and σ_{DS} is derived at the end of this section. The variable z_n' is a uniform random variable in the interval 0 to 1.2μs. These variables are sorted in descending order, i.e., $\tau_N' > \tau_{N-1}' > \cdots > \tau_1'$.

According to this definition, $\tau_1' = 0$. The delay from the n_{th} path, denoted by τ_n, is then quantized according to (2.4):

$$\tau_n = \frac{T_C}{16} \left\lfloor \frac{\tau_n' - \tau_1'}{\frac{T_C}{16}} + \frac{1}{2} \right\rfloor, \tag{2.4}$$

where T_{C} is the duration of a chip interval.

Chapter 3

Channel Estimation

3.1 The Estimation Problem

In a real-world environment, the transmission channel used by a communication system is not stationary and undergoes changes with time, sometimes rapidly. Such a channel can be modeled by (2.3). To establish reliable communication, the MIMO methods explained in the previous chapter can be utilized for the communication systems if the channel is known; see Section 2. However, three difficulties arise when the channel is required by the communications system:

1. Channel knowledge must be acquired by the receiver (channel estimation)

2. The channel knowledge must be fed back to the transmitter (see Chapter 4)

3. If the channel changes significantly, the channel knowledge at the transmitter becomes inaccurate and outdated, this is known as *data aging*. (We do not consider this issue here.)

Channel estimation is a fundamental operation required by every communication system. For this reason,this entire chapter is devoted to the basis of estimation algorithms. Estimation is typically done in three ways: filtering, smoothing and prediction. Filtering and prediction are real-time operations. Filtering at time t is done using data received prior to time t. Prediction is estimation of the process at time $t + \tau$ using data measured at time t and earlier. Second-order statistics (i.e., mean and correlation functions) of signals and noise are required in this computation. The main approach to the filtering problem, i.e., channel estimation, is the minimization of mean-square errors. This error is defined as the power difference between the desired response and the filter output.

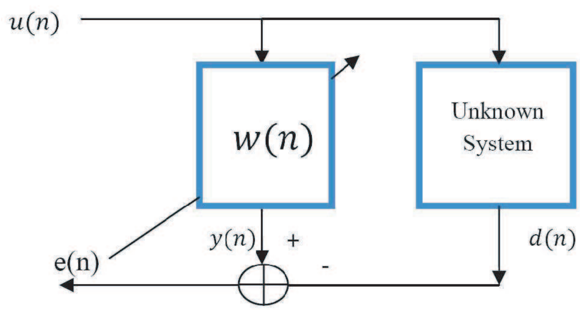

Figure 3.1: Filtering system block diagram.

Linear filtering is sufficient for the task of channel estimation as long as the channel is stationary (Wiener filtering is optimal for stationary channels; see Section 3.2). However, estimation becomes more challenging for dynamic environments. More complex algorithms, such as recursive least squares (RLS) and Kalman filters, are the alternative techniques for estimating the channel in wireless communication systems.

This chapter discusses the fundamentals of tracking algorithms, such as the Wiener filter. The Wiener filter is the optimum tool for the estimation problem in stationary environments. Next, the steepest descent method and its relation to Wiener filter algorithm is studied. At the end, the least mean squares (LMS) method is identified as the most practical estimation algorithm due to its low computational complexity and its independence of a priori knowledge of the channel statistics.

3.2 Wiener Filter

A large number of estimation algorithms have been developed to track the channel changes during the last century. These tools are known as adaptive filters. Adaptive filters are not unique to MIMO communication, but are commonly used in the field of signal processing. The Wiener filter is the optimum linear discrete-time filter and is specified in terms of its impulse response [21]. The optimum filter is the one which minimizes the cost function, here the power difference between the actual process and the filter's estimation. Fig. 3.1 shows a system block diagram of an identification system, where $d(n)$ is the desired response and $y(n)$ is the estimated output or filter output.

This system can be seen either as plant identification or filtering. We concentrate our study on the former concept and begin with the design of the optimum filter. For optimization of the identification filter, the cost function should be minimized. The cost function is the mean-square value of the estimation error which is defined as the difference between the desired output and the filter output. Minimum mean square estimation (MMSE) leads to a set of equations known as the Wiener-hopf equations to be discussed shortly. In practice, solution of these equations requires second-order statistical knowledge of the channel, which increases the computational complexity. Different mathematical approaches have been employed to solve for Wiener-hopf equation and simplify the procedures. Two approaches are considered which lead to tractable mathematics. One is the principle of orthogonality, and the other is the error performance surface.

3.2.1 Principle of Orthogonality

Considering the block diagram shown in Fig. 3.1, the output of the unknown system is estimated by

$$y(n) = \sum_{k=0}^{L-1} w_k^* u(n-k) \tag{3.1}$$

which illustrates an inner product of the filter coefficients w_k and the system input $u(n-k)$. The filter input and the desired response are assumed to be jointly wide-sense stationary stochastic processes with zero mean. Then, the estimation error is the random sample of time n given by

$$e(n) = d(n) - y(n) \tag{3.2}$$

and the cost function is defined in (3.3), realizing that the input data and the filter coefficients are complex values:

$$J = \mathbb{E}[e(n)e^*(n)] = \mathbb{E}[|e(n)|^2] \tag{3.3}$$

Solving for optimization, the cost function needs to be minimized. In that case, a gradient operator is used to migrate towards the stationary point of the cost function:

$$\nabla_k(J) = -2\ \mathbb{E}[u(n-k)e^*(n)]; \quad k = 1, 2, ..., L. \tag{3.4}$$

Equating (3.4) to zero gives necessary and sufficient condition for J to attain its minimum value. Note that the kth derivative is taken with respect to w_k. Therefore, the corresponding value of $e(n)$ must be orthogonal to each input sample, where orthogonality between two sequences of $\mathbf{u}$ and $\mathbf{v}$ is defined as $\mathbb{E}[\mathbf{u}(n)\mathbf{v}^*(n)]$. Using this orthogonality principle, the correlation between the filter outputs $y(n)$ and error estimation can be expressed as

$$\mathbb{E}[y(n)e^*(n)] = \sum_{k=0}^{L-1} w_k^* \mathbb{E}[u(n-k)e^*(n)]$$

This implies that the estimated outputs $y(n)$ and the corresponding estimation error $e(n)$ are orthogonal as well. In this approach, we substitute equations (3.1) and (3.2) into

$$\mathbb{E}[u(n-k)e^*(n)] = 0, \quad k = 0, 1, 2, \ldots, L-1$$

to obtain

$$\mathbb{E}[u(n-k)(d^*(n) - \sum_{i=0}^{L-1} w_{oi} u^*(n-i))] = 0, \quad k = 0, 1, 2, \ldots, L-1$$

or

$$\sum_{i=0}^{L-1} w_{oi} \mathbb{E}[u(n-k)u^*(n-i)] = \mathbb{E}[u(n-k)d^*(n)]. \quad k = 0, 1, 2, \ldots, L-1 \tag{3.5}$$

Defining terms as:

$$r(i-k) = \mathbb{E}[u(n-k)u^*(n-i)] \tag{3.6}$$

$$p(-k) = \mathbb{E}[u(n-k)d^*(n)] \tag{3.7}$$

where (3.6) is the auto-correlation of the filter inputs and (3.7) is the cross-correlation between the filter input and the desired response (output of the unknown system).

Therefore, equation (3.5) can be rewritten as

$$\sum_{i=0}^{L} w_{oi} r(i-k) = p(-k), \quad k = 0, 1, 2, \ldots, L-1$$

These are the so-called Wiener-Hopf equations, which can be solved efficiently based on spectral factorization. Another approach can be taken to tackle this problem. Using (3.2) and (3.3),

$$e(n) = d(n) - \sum_{k=0}^{L-1} w_k^* u(n-k),$$

and

$$J = \mathbb{E}[|d(n)|^2] - \sum_{k=0}^{L-1} w_k^* \mathbb{E}[u(n-k)d^*(n)] - \sum_{k=0}^{L-1} w_k \mathbb{E}[u(n-k)d(n)] + \sum_{k=0}^{L-1}\sum_{i=0}^{L-1} w_k^* w_i \mathbb{E}[u(n-k)u^*(n-i)]$$

The above equation can be simplified to

$$J = \sigma_d^2 - \sum_{i=0}^{L-1} w_k^* p(-k) - \sum_{i=0}^{L-1} w_k p^*(-k) + \sum_{i=0}^{L-1} w_k^* w_i r(n-i)$$

which implies that the cost function is a second-order function of the filter tap-weights. The dependence of the cost function on the tap weights can be visualized as a bowl-shaped, $L+1$-dimensional surface with L degrees of freedom. At the bottom of the error-surface, the cost function attains its minimum value. This can be represented as follows:

$$\nabla_k(J) = \frac{\partial J}{\partial a_k} + j\frac{\partial J}{\partial b_k} \tag{3.8}$$

where a_k and b_k are real and imaginary components of w_k. Then,

$$\nabla_k(J) = -2p(-k) + 2\sum_{i=0}^{L-1} w_i r(i-k)$$

The optimal point is reached when $\nabla_k = 0$, or equivalently,

$$p(-k) = \sum_{i=0}^{L-1} w_{oi} r(i-k), \quad k = 0, 1, 2, \ldots$$

which is equivalent to Wiener-Hopf equation.

We have shown that, in order to come up with an optimum system, different approaches may be taken. Applying the gradient operation over the cost function results in an optimum filter, and its performance will be studied over the error performance surface. In this approach, it has also been proved that the estimation error is orthogonal to the actual output of the filter.

3.3 Methods of Steepest Descent (SD) and LMS Algorithm

To set up the problem in the context of this thesis, a filter which is less complex and more robust to fast changes - in our case, the channel - is our primary interest.

The goal is to track the channel in order to generate a sufficiently good estimate of the channel statistics, which can then be used to predict the channel's future behavior. The SD technique belongs to the family of iterative methods of optimization and it provides a method of searching for a multidimensional *performance surface*. This is a gradient-based method which means that the algorithm follows the local gradient. The steepest descent method is therefore a recursive algorithm which starts from some initial value of the solution, and it tends to improve with the number of iterations. SD is akin to a multiparameter closed-loop deterministic control system which finds the minimum-point of the error-performance surface without knowledge of surface itself, giving basic clues that lead to the development of the LMS algorithm.

3.3.1 The SD Algorithm

The input sequence to our system, $u(n), u(n-1), \ldots, u(n-M+1)$ is assumed to be a wide-sense stationary stochastic process of zero-mean and correlation matrix $\mathbf{R}$. The corresponding desired response at the filter output is denoted by $y(n) = \mathbf{w}^H(n)\mathbf{u}(n)$ and the filter tap-weights are $w_n, w_1, ..., w_{n-M+1}$. Note that the input vector $\mathbf{u}(n)$ and $d(n)$ are assumed to be jointly stationary.

Applying 3.2 the cost function is:

$$J(n) = \sigma_d^2 - \mathbf{w}^H(n)\mathbf{p} - \mathbf{p}^H\mathbf{w}(n) + \mathbf{w}^H(n)\mathbf{R}\mathbf{w}(n)$$

which is equivalent to the estimation of the mean square error to be minimized.

As has been already mentioned, the cost function is quadratic in the tap-weight vector. The error performance surface is a visualization of the dependence of the mean-squared error on the elements of the vector $\mathbf{w}(n)$ as a bowl shape. An adaptive process continually seeks the bottom or minimum point of this surface. Let $\mathbf{w}_0$ be the optimal solution defined by *Wiener-hopf equations*:

$$\mathbf{R}\mathbf{w}_0 = \mathbf{p}$$

Therefore, the minimum value of the cost function can be followed:

$$J_{\min} = \sigma_d^2 - \mathbf{p}^H\mathbf{R}^{-1}\mathbf{p}$$

where

$$\sigma_y^2 = \mathbb{E}[\mathbf{w}_0^H\mathbf{u}(n)\mathbf{u}^H(n)\mathbf{w}_0] = \mathbf{w}_0^H\mathbb{E}[\mathbf{u}(n)\mathbf{u}^H]\mathbf{w}_0$$

and

$$J_{\min} = \sigma_d^2 - \sigma_y^2$$

.

The algorithm for SD is obtained as follows:

1. Start the algorithm with an initial $\mathbf{w}_0$ which can be set to zero.

2. Evaluate the gradient from (3.8).

3. Compute the next tap-weight vector by making a change in the initial or present vector in a direction opposite to that of the gradient vector. This is done as

$$\mathbf{w}(n+1) = \mathbf{w}(n) + \frac{1}{2}\,[-\nabla(J(n))], \tag{3.9}$$

One half is the step size parameter which helps the algorithm to converge faster.

4) Go back to step 2.

The gradient in (3.9) is given by

$$\nabla(J(n)) = -2\mathbf{p} + 2\mathbf{R}\mathbf{w}(n),$$

and

$$\mathbf{w}(n+1) = \mathbf{w}(n) + [\mathbf{p} - \mathbf{R}\mathbf{w}(n)],$$

which $\mathbf{p} - \mathbf{R}\mathbf{w}(n)$ is the correction weight vector.

Note that, from (3.4),

$$\mathbb{E}[\mathbf{u}(n)e^H(n)] = -\nabla(J(n)) = -\nabla(\mathbb{E}[e(n)e^H(n)]). \tag{3.10}$$

This shows that at $J_{\min}$, input sequence $\mathbf{u}(n)$ is orthogonal to the error sequence.

3.3.2 Stochastic Gradient-Based Algorithms: the LMS Approach

One of the most important features of stochastic gradient-based algorithms (SGBA) e.g. the LMS algorithm, is their simplicity. In the LMS algorithm, measurement of the correlation function and the performance of matrix inversion is not required. The value of the tap-weight vector $\hat{\mathbf{w}}(n)$ using LMS represents an estimate of $\mathbf{w}(n)$ whose expected value approaches the Wiener filter ($\mathbf{w}_0$), for a wide-sense stationary (WSS) process as n approaches infinity.

In the LMS algorithm an approximation to (3.10) is used to compute $\mathbf{w}(n+1)$ from $\mathbf{w}(n)$

$$\mathbf{u}(n)e^*(n) = \hat{\mathbf{w}}(n+1) - \hat{\mathbf{w}}(n) = \delta\hat{\mathbf{w}}(n).$$

Basically, the LMS algorithm avoids the operation of expectation. For this reason, it is a less complex and is the most widely used algorithm. In the LMS algorithm, the tap-weight vector $\hat{\mathbf{w}}(n)$ is not exactly the one which will be evaluated from the SD algorithm. $\hat{\mathbf{w}}(n)$ executes a random motion around the minimum point of the error performance surface, which requires the step-size-parameter μ to satisfy conditions related to the eigenvalues of the random correlation matrix $\mathbf{R}$ of the tap-inputs. In the LMS algorithm, an adaptive mechanism is utilized in place of a deterministic approach in SD. This way, there is a penalty for misadjustment given by ratio $J_{\text{LMS}}(\infty)/J_{\text{SD}}$ This leads to the following:

1. The LMS converges to the mean $\mathbb{E}[\hat{\mathbf{w}}(n)] = \mathbf{w}_0$, which is the Wiener solution as $n \to \infty$
2. The LMS converges to the mean square $J_{\text{LMS}}(n) \to J_{\text{SD}}(\infty)$ as $n \to \infty$

As was shown earlier, the exact solution of $\nabla(J(n))$ leads to the Wiener solution $\mathbf{w}_0$, however it needs a priori knowledge of $\mathbf{R}$ (*the autocorrelation of the tap inputs)* and $\mathbf{p}$ (*the cross correlation of u and d*). The LMS algorithm estimates the gradient from instantaneous data. In other words, the tap-weight vector is updated in accordance with an algorithm that adapts to the incoming data instead of measurement of $\mathbf{R}$ and $\mathbf{p}$, which are estimated as

$$\hat{\mathbf{R}}(n) = \mathbf{u}(n)\mathbf{u}^H(n),$$

and

$$\hat{\mathbf{p}}(n) = \mathbf{u}(n)d^*(n),$$

Therefore,

$$\nabla J_{\text{LMS}}(n) = -2\mathbf{u}(n)d^*(n) + 2\mathbf{u}(n)\mathbf{u}^H(n)\hat{\mathbf{w}}(n).$$

This shows that the estimation is biased since the tap-weight vector $\hat{\mathbf{w}}(n)$ is a random vector that depends on the vector $u(n)$. The recursive relation for computing the tap-weight vector is finally given by

$$\hat{\mathbf{w}}(n+1) = \hat{\mathbf{w}}(n) + \mu\mathbf{u}(n)[d^*(n) - \mathbf{u}^H(n)\hat{\mathbf{w}}(n)]$$

and μ is constrained by $0 < \mu < 2/\text{total input power}$.

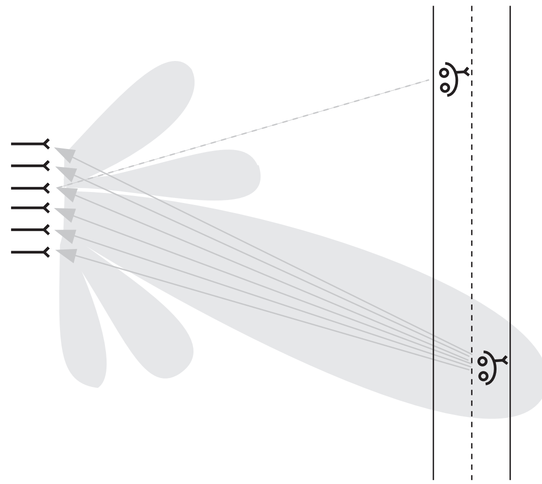

Figure 3.2: Uplink transmission scenario. Two vehicles are approaching one another, each at a speed of 60km/h.

Summary of the LMS Algorithm

In practice, the LMS algorithm is regarded as a reliable approach for channel estimation; however, the channel changes are required to be slower than the speed of LMS operation. Indeed, the LMS algorithm never reaches the solution of SD algorithm

$$\mathbb{E}[J_{\text{LMS}}(n)] \neq \mathbb{E}[J_{\text{SD}}(n)].$$

The LMS algorithm can be summarized as follows:

$$e(n) = d(n) - \hat{\mathbf{w}}^H(n)\mathbf{u}(n) \tag{3.11}$$

$$\hat{\mathbf{w}}(n+1) = \hat{\mathbf{w}}(n) + \mu\mathbf{u}(n)e^*(n) \tag{3.12}$$

3.4 Example: Channel Estimation in the MIMO Scenario

We examine a scenario in this section to investigate the performance of the LMS algorithm in a time-varying MIMO channel environment; see Fig. 3.2. Another example is dedicated to channel estimation for the LTE environment, which is given in Section 4.4.1.

The presence of known pilots $\mathbf{P}$ is considered throughout this thesis for the purpose of channel estimation. The pilot scheme can be selected from a variety of methods. We restrict our choice to the embedded spread-spectrum pilot discussed in [22]. The concept of embedded pilot was first introduced in [23] for SISO systems,

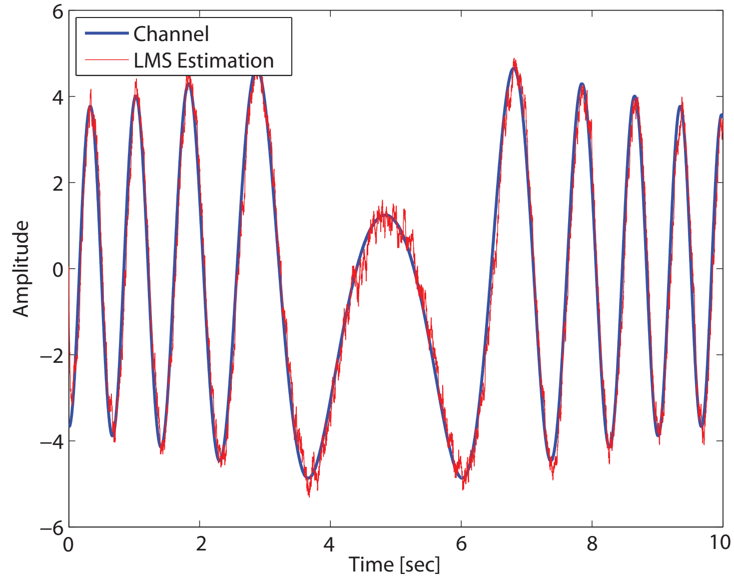

Figure 3.3: LMS channel tracking for the reference transmitter.

and later extended to multicarrier systems in [24]. Pilot embedded scheme is superior to the conventional pilot scheme in a number of ways. The concept of conventional pilot transmission is to time-multiplex pilot along with the data symbol [25]. This concept fails in the tracking of the channel with very low SNR and a fast fading rate. In that case, a large number of pilots is needed, which is not bandwidth efficient. However, in the pilot embedded scheme, the system acquires the necessary channel information at the cost of much smaller pilot energy and bandwidth wastage. For a transmitted pilot sequence of $\mathbf{P}$, the channel can be estimated by minimizing a cost function, as shown in Fig. 3.3:

$$J\left(\hat{\mathbf{H}}\right) = \mathbb{E}\left[\left\|\hat{\mathbf{H}}\mathbf{P} - \mathbf{y}\right\|^2\right]. \tag{3.13}$$

Taking partial derivatives with respect to the entries of $\hat{\mathbf{H}}$ leads to the *Principle of Orthogonality* (see Section 3.2.1) of optimal linear estimation

$$\mathbb{E}\left[\left(\hat{\mathbf{H}}\mathbf{P} - \mathbf{y}\right)\mathbf{y}^*\right] = 0,$$

from which we obtain

$$\hat{\mathbf{H}} = \mathbb{E}\left[\mathbf{y}\mathbf{y}^*\right]\mathbb{E}\left[\mathbf{P}\mathbf{y}^*\right]^{-1}. \tag{3.14}$$

A proper pilot signal selection is needed for the inverse to exist. The basic idea of the LMS can be applied here and the error computation can be evaluated by

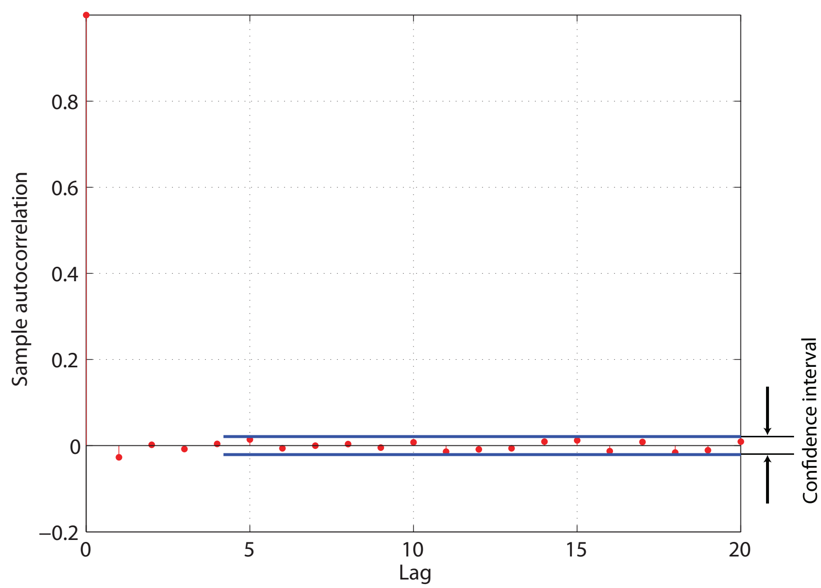

Figure 3.4: Autocorrelation function of the residual error of the LMS channel estimation.

(3.3). However, in order to avoid the inverse in (3.14), the steepest descent method (see Section 3.3) is used to update the estimate from the error as

$$\hat{\mathbf{H}}(n+1) = \hat{\mathbf{H}}(n) + \mu\mathbb{E}\left[\left(\mathbf{y}(n) - \hat{\mathbf{H}}(n)\mathbf{P}(n)\right)\mathbf{P}(n)^{+}\right],$$

where the sample time n is any convenient discrete sample time, equal to or slower than the signal sampling rate. The expectation $\mathbb{E}\left[\left(\mathbf{y}(n) - \hat{\mathbf{H}}(n)\mathbf{P}(n)\right)\mathbf{P}(n)^{+}\right]$ can be evaluated in a variety of ways, the simplest being the one-step approximation leading to

$$\hat{\mathbf{H}}(n+1) = \hat{\mathbf{H}}(n) + \mu\left(\mathbf{y}(n) - \hat{\mathbf{H}}(n)\mathbf{P}(n)\right)\mathbf{P}(n)^{+}.$$

In order to avoid stability problems, the LMS algorithm is typically *normalized* and the basic algorithm used is

$$\hat{\mathbf{H}}(n+1) = \hat{\mathbf{H}}(n) + \mu\frac{\left(\mathbf{y}(n) - \hat{\mathbf{H}}(n)\mathbf{P}(n)\right)\mathbf{P}(n)^{+}}{\mathbf{P}^{+}(n)\mathbf{P}(n)}.$$

Note that the choice of unit power pilot avoids the normalization.

In the uplink scenario illustrated in Fig. 3.2, the BS has $N = 5$ antennas, spaced 90cm from each other. The two transmitters are moving towards each other at the speed of 60km/h. The signals are transmitted over the carrier frequency of 1.8GHz by two vehicles which are traveling 100m away from the receiver.

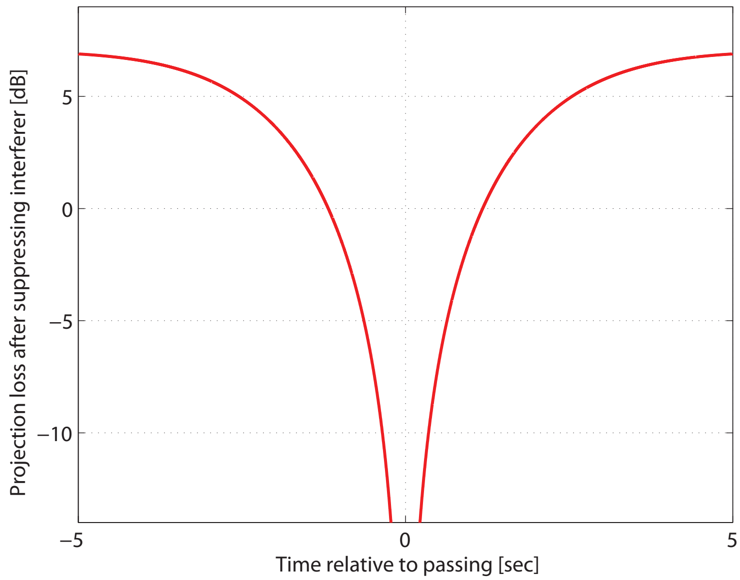

Figure 3.5: Projection loss for two passing transmitters.

Let us assume that vehicle two is the interferer to vehicle one. Thus, Fig. 3.3 shows the channel estimation for vehicle one at the BS. The simple LMS algorithm (3.11), with $\mu = 0.02$ and SNR (power of pilots to noise) of 4dB, is considered. Pilots are transmitted every 1ms to the receiver from each user. For example, each HSDPA packet traveling duration is 2ms, which can be regarded as 2 pilots per packet. In that case, the error between the received signal and the transmitted signal is reduced by approximately $(10 \log |0.04| =)13.6$dB.

Regardless of the magnitude of the error, another way to verify the estimation accuracy is to compute the statistics of the residual error (3.2). Basically, the autocorrelation of residual error is random and has a normal distribution. Fig. 3.4 shows that all the autocorrelation samples are within a well-defined confidence interval. This indicates that the estimation is independent of the system's characteristics and is reliable. We consider 95% confidence interval which is shown by horizontal lines in Fig. 3.4. This is somewhat consistent with the principle of orthogonality which has been discussed earlier in Section 3.2.1. It is clear from Fig. 3.5 that null-steering fails to suppress the interference by the second vehicle when they are passing each other; see Section 2.2. The channel is assumed to be perfectly known at the BS, which is known as perfect CSIR. However, Fig. 3.6 represents the projection loss due to null-steering when the channel is estimated by the LMS algorithm. This also verifies that LMS algorithm is a suitable tool for channel estimation in practical

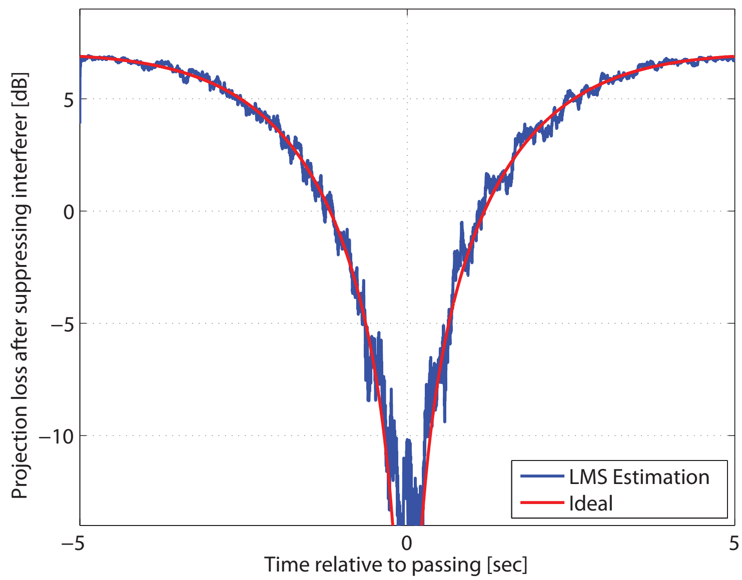

Figure 3.6: Projection loss for two passing transmitters where the LMS is used to estimate the interfering channel with samples taken every 1ms.

implementations. However, the LMS algorithm is relatively slow in adapting to the changes of the channel and therefore, its parameters needs to be chosen as a function of Doppler speed, 10.8Hz in this example.

Chapter 4

Channel State Information Feedback and Quantization

Knowledge of the parameters of the wireless channel at the transmitter side is crucial for establishing reliable communication at rates close to the channel capacity. Changes in the channel response caused by mobility of the transmitter and receiver and evolution of the signal propagation environment require adaptation of the transmission strategy. Knowledge of the channel state information (CSI) obtained by the receiver using channel estimation techniques needs to be communicated back to the transmitter via a feedback channel. Due to errors in channel estimation and the limitations of the feedback channel, the transmitter often needs to operate in the presence of imperfect CSI. This is particulary important for communications over multiple antenna channels where transmission can be very sensitive to CSI errors.

4.1 Finite-Rate Feedback of CSI

The concept of channels with feedback was introduced by Shannon [26] and an enormous amount of research effort has been dedicated to applications of this concept to various wireless communication systems. Although the capacity of the feedback channel remains unknown for the general case, feedback is widely used in practical communications. Particularly, in 3G and 4G cellular standards feedback of the signal-to-interference and noise ratio (SINR) conditions of the mobile station is used for rate adaptation at the transmitter and even feedback of information about the channel matrix is used for transmission in MIMO modes.

Cellular networks with a single-antenna BS achieve their highest throughput using scheduling techniques, where each MS is required to feed back its SINR condition to the BS. In order to reduce the feedback traffic on the uplink channel, applying a predetermined threshold for sending back the SINR condition has been proposed [27] together, with a large number of other user selection algorithms considering limited feedback and targeting optimization of various quality parameters. Shared feedback resources were first studied in [28] which considers a shared random access feedback channel. Also, in [29], another technique where users can compete for resources in a limited feedback channel is discussed. A number of theoretic results for channels with limited feedback have been obtained. For example, in [30] the capacity of a broadcast channel with finite-rate feedback is computed.

For cellular networks with multiple antennas at the BS, single user (opportunistic) or multiuser MIMO (MU-MIMO) downlink transmission can be utilized and antenna array gains can be expected; see Section 1.2. Efficient communication over MIMO channels requires knowledge of the channel matrix at the transmitter; see Section 1.2. Particularly this knowledge is required for the optimal power allocation scenario that maximizes the mutual information of the MIMO channel and is achieved through waterfilling over the channel singular values [31]. Linear precoding methods, including beamforming, require transmitter channel state information (CSIT) as well. Similarly, efficient operation in the MU-MIMO scenario happens primarily when precoding is applied at the BS to minimize the cross-interference between the data streams directed to the MS users. Due to the limitations of the feedback channel, CSI feedback is mostly accomplished in a quantized form where the receiver approximates the channel vector (for single-antenna MS) by a codeword from a codebook, which is known to both transmitter and receiver [32]. The index of the codeword is then communicated from the receiver to the transmitter via the feedback link.

One of the fundamental research questions is to quantify the throughput loss which is experienced by a system using quantized CSI feedback to the ideal theoretic case of full CSI. The amount of quantization and feedback is quantified in terms of the number of quantization bits. It has been shown that even a small amount of feedback is proven to be beneficial [33, 34] and provides sizable gains over no-CSI cases. However, [32] demonstrated that the number of feedback bits should be on the order of the number of transmit antennas M at the BS and log(SINR) experienced by MS users to maintain a constant gap between the sum-rate of the ideal CSIT case and the realistic case with quantization. Section 4.2 discusses the above problem in detail and illustrates theoretic results.

Evidently, the choice of quantization methods also affects the performance of the quantized system. Many techniques have been proposed for quantization of the channel vectors; among these are the random vector quantization (RVQ) and Grassmannian line packing [35]; see Section 4.3. We also note that channel estimation at the receiver side is not error-free; there are also delays in feeding back the CSI information. Therefore, a significant number of research contributions have been dedicated to designing codebooks and analyzing, and to frequency of the CSI feedback. Section 4.4.1 discusses joint channel estimation and quantized feedback.

4.2 Feedback Quantization for Multiuser MIMO, Problem Definition and Approach

Channel state information in flat fading MIMO channels consists of two components (a) Channel quality information (CQI), which carries the information regarding the channel's SINR, and (b) Channel direction information (CDI), which carries the information regarding the direction of the channel vector.

In the present discussion we limit our consideration to quantization and feedback of CDI assuming perfect knowledge of CQI. We consider the downlink communication scenario and assume that the BS is equipped with M antennas and is sending $K \leq M$ independent data streams to K users. Each MS is equipped with a single antenna. It has been shown in [30] that in the case a BS that is serving a number of MSs that is smaller than or equal to the number of transmit antennas at the BS, the knowledge of the magnitude of CSI is not required.

Let the composite downlink channel matrix be

$$\mathbf{H}^{\dagger} = [\mathbf{h}_1 \ \mathbf{h}_2 \ \cdots \ \mathbf{h}_K]$$

where $\mathbf{H}$ has dimension $K \times M$. The signal received by the ith MS is

$$y_i = \mathbf{h}_i^{\dagger}\mathbf{x} + \eta_i, \quad i = 1, 2, \ldots, K \tag{4.1}$$

where $\mathbf{h}_i \in C^{M\times 1}$ and $\mathbf{x} \in C^{M\times 1}$ is the transmitted signal. We consider linear precoding where the transmitter multiplies the symbol intended for each user (MS) by a beamforming vector and transmits the sum of these vectors to the users. Let us denote the symbol intended for the ith user by s_i and the corresponding unit norm beamforming vector by ν_i. Then the transmitted signal is

$$\mathbf{x} = \sum_{i=1}^{K} s_i \nu_i$$

and therefore, the signal (4.1) received by the ith user is

$$y_i = \mathbf{h}_i^{\dagger} \mathbf{x} + \eta_i = \mathbf{h}^{\dagger}{}_i \sum_{i=1}^{K} s_i \nu_i + \eta_i.$$

Typically ZF beamforming is used as the precoding scheme, meaning that the beamforming vectors ν_i are chosen to be the normalized columns of $\mathbf{H}^*(\mathbf{H}\mathbf{H}^*)^{-1}$ (see 1.2). The precoding matrix is designed to orthogonalize the signals transmitted to the users. However, this orthogonalization cannot be perfect since the knowledge of channel matrix $\mathbf{H}^{\dagger}$ is incomplete: information sent from MS to BS via the feedback channel must be quantized and therefore carries inherent quantization errors. We assume that the BS has obtained an estimate $\hat{\mathbf{H}}$ of the matrix $\mathbf{H}$. This estimate is formed by K vectors $\hat{\mathbf{h}}_i$ received via feedback from the K users. We assume that ith MS uses B_i bits to quantize its $1 \times M$ channel vector $\mathbf{h}_i^{\dagger}$.

Let us consider the Rayleigh fading channel $\mathbf{H}$ and assume that random vector quantization is performed at every MS to quantize the channel information. It has been shown in [32] that for random vector quantization of Gaussian vectors, the average quantization error is upper bounded as

$$\mathbb{E}_{H,W}\left[\sin^2\left(\angle\left(\hat{\mathbf{h}}_i, \tilde{\mathbf{h}}_i\right)\right)\right] < 2^{-\frac{B_i}{M-1}} . \tag{4.2}$$

where $\tilde{\mathbf{h}}_i = \frac{\mathbf{h}_i}{\|\mathbf{h}_i\|}$ and the expectation is taken over the channel realizations and the quantization codebooks.

We make the assumption that P_{t_i} is the allocated signal power on the data stream transmitted to the ith MS. The SINR at the ith MS (see (4.1)) can be evaluated as:

$$\text{SINR}_i = \frac{P_{t_i}|\mathbf{h}_i^{\dagger}\nu_i|^2}{1 + \sum_{j\neq i} P_{t_j}|\mathbf{h}_i^{\dagger}\nu_j|^2}. \tag{4.3}$$

We assume that precoding vectors ν_i are the columns of the ZF beamforming matrix $\hat{\mathbf{H}}^*(\hat{\mathbf{H}}\hat{\mathbf{H}}^*)^{-1}$ constructed using quantized channel matrix $\hat{\mathbf{H}}^{\dagger}$. It has been shown in [32] that the residual interference terms in the denominator of (4.3) can be upperbounded as

$$\mathbb{E}_{H,W}\left[\sin^2\left(\angle\left(\hat{\mathbf{h}}_i, \nu_j\right)\right)\right] \quad < \quad 2^{-\frac{B_i}{M-1}} . \tag{4.4}$$

We now compare the sum-rate capacity of the ideal ZF beamforming case and the sum-rate with ZF beamforming based on quantized feedback information. We follow the lines of derivation in [32] but consider the unequal power case. The sum-rate for the ideal ZF case is equal to

$$R_{\mathrm{ZF}}\left(P_{t_1},\dots P_{t_k},B_1,\dots B_k\right) \;=\; \sum_{i=1}^{K}\mathbb{E}_H\left[\log_2\left(1+P_{t_i}|\mathbf{h}_i^\dagger\nu_{\mathrm{ZF},i}|^2\right)\right]$$

where $\nu_{\mathrm{ZF},i}$ is orthogonal to $\mathbf{h}_j$, $j\neq i$. The rate for the quantized case is

$$\begin{aligned}
R_{\mathrm{FB}}\left(P_{t_1},\dots P_{t_K},B_1,\dots B_K\right) &= \sum_{i=1}^{K}\mathbb{E}_{H,W}\left[\log_2\left(1+\mathrm{SINR}_i\right)\right]\\
&= \sum_{i=1}^{K}\mathbb{E}_{H,W}\left[\log_2\left(1+\frac{P_{t_i}|\mathbf{h}_i^\dagger\nu_i|^2}{1+\sum_{j\neq i}P_{t_j}|\mathbf{h}_i^\dagger\nu_j|^2}\right)\right]\\
&= \sum_{i=1}^{K}\mathbb{E}_{H,W}\left[\log_2\left(1+P_{t_i}|\mathbf{h}_i^\dagger\nu_i|^2+\sum_{j\neq i}P_{t_i}|\mathbf{h}_i^\dagger\nu_j|^2\right)\right]\\
&\quad +\sum_{i=1}^{K}\mathbb{E}_{H,W}\left[\log_2\left(1+\sum_{j\neq i}P_{t_i}|\mathbf{h}_i^\dagger\nu_j|^2\right)\right]\\
&\leq \sum_{i=1}^{K}\mathbb{E}_{H,W}\left[\log_2\left(1+P_{t_i}|\mathbf{h}_i^\dagger\nu_i|^2\right)\right]\\
&\quad +\sum_{i=1}^{K}\mathbb{E}_{H,W}\left[\log_2\left(1+\sum_{j\neq i}P_{t_i}|\mathbf{h}_i^\dagger\nu_j|^2\right)\right]
\end{aligned}$$

We start upper bounding the difference between rates

$$\begin{aligned}
\Delta\mathrm{R}\left(P_{t_1},\dots P_{t_K},B_1,\dots B_K\right) &= R_{\mathrm{ZF}}\left(P_{t_1},\dots P_{t_K},B_1,\dots B_K\right)\\
&\quad - R_{\mathrm{FB}}\left(P_{t_1},\dots P_{t_K},B_1,\dots B_K\right)\\
&\leq \sum_{i=1}^{K}\mathbb{E}_{H,W}\left[\log_2\left(1+\sum_{j\neq i}P_{t_j}|\mathbf{h}_i^\dagger\nu_j|^2\right)\right]
\end{aligned}$$

observing that

$$\mathbb{E}_H\left[\log_2\left(1+P_{t_i}|\mathbf{h}_i^\dagger\nu_{\mathrm{ZF},i}|^2\right)\right]=\mathbb{E}_{H,W}\left[\log_2\left(1+P_{t_i}|\mathbf{h}_i^\dagger\nu_i|^2\right)\right]\ .$$

Using (4.2), (4.4), and Jensen's inequality assuming $\mathbb{E}\left(\|h_k\|^2\right)=M$, we obtain

$$\Delta\mathrm{R}\left(P_{t_1},\dots P_{t_K},B_1,\dots B_k\right) \;\leq\; \sum_{i=1}^{K}\log_2\left(1+\frac{M}{M-1}P_{t_i}2^{-\frac{B_i}{M-1}}\right) \qquad (4.5)$$

$\frac{1}{\sqrt{2}}$ $\frac{1}{\sqrt{2}}$ 0	$\frac{1}{\sqrt{2}}$ 0 $\frac{1}{\sqrt{2}}$	0 $\frac{1}{\sqrt{2}}$ $\frac{1}{\sqrt{2}}$	$\frac{1}{\sqrt{2}}e^{2\pi j/3}$ $\frac{1}{\sqrt{2}}e^{4\pi j/3}$ 0
$\frac{1}{\sqrt{2}}e^{2\pi j/3}$ 0 $\frac{1}{\sqrt{2}}e^{4\pi j/3}$	$\frac{1}{\sqrt{2}}e^{4\pi j/3}$ 0 $\frac{1}{\sqrt{2}}e^{2\pi j/3}$	$\frac{1}{\sqrt{2}}e^{4\pi j/3}$ $\frac{1}{\sqrt{2}}e^{2\pi j/3}$ 0	0 $\frac{1}{\sqrt{2}}e^{4\pi j/3}$ $\frac{1}{\sqrt{2}}e^{2\pi j/3}$

Table 4.1: Grassmannian generated codebook for $M = 3$ and $N = 2^3 = 8$.

For the case of equal power data streams, i.e. $P_{t_i} = P_t/M$, $i = 1, 2, \ldots, K$, and the numbers of bits $B_i = B$, $i = 1, 2, \ldots, K$ (4.5) simplifies to

$$\Delta\mathrm{R}\left(P_t, \ldots P_t, B, \ldots B\right) \quad \leq \quad K \log_2\left(1 + \frac{M}{M-1} P_t 2^{-\frac{B}{M-1}}\right) \tag{4.6}$$

and leads to the formula for the number of bits [32]

$$B = (M-1)\log(P_t, 2) \approx \frac{M-1}{3} P_{t_{\mathrm{dB}}} \tag{4.7}$$

required to get a constant gap between the ideal and quantized performances. In the case where the fixed number of bits B is used the SINR_i values will saturate at some constant level, as can be seen from (4.3).

Looking at (4.5) we notice that in order to balance the terms on the right hand side (i.e., making them equal) we need

$$P_{t_i}\ 2^{-\frac{B_i}{M-1}} \approx P_{t_j}\ 2^{-\frac{B_j}{M-1}} \quad i \neq j \tag{4.8}$$

This means that users with smaller SINR need fewer feedback bits and users with higher SINR need more bits to maintain the same scaling of the gap from the ideal ZF beamforming rate.

4.3 Codebook Design

Codebook design is an important component in feedback quantization. Quantization error can be reduced by increasing the codebook size. As a result, optimal, perfect CSI performance can be approached at the cost of compromising data transmission rate in the opposite direction. Feedback information itself becomes sensitive to errors if the amount of feedback bits is increased significantly. Therefore, it is essential not to use an excessively high feedback rate to optimize a system's performance [36].

The aim of codebook design is to select a quantization method which would deliver the best performance given the number of feedback bits used. Codebook design and quantization methods can be broadly classified into two categories: methods where quantization vectors are designed based on training data sets such as Random Vector Quantization, and methods based on geometric codebook design which are independent of the possible data sets such as Grassmanian subspace packing.

Grassmannian subspace packing is a most often used codebook design in precoding schemes, mostly due to the lack of a priori channel knowledge. In the case of training availability, better codebooks can be acquired. For instance, [37] proposed a vector quantizer based on the LBG algorithm and use of chordal distance which outperforms quantizer based on Grassmannian codebooks. While most work in the area of codebook design have been devoted to the static channels, dynamic codebook adaptation has also been considered recently in [38, 39].

4.3.1 Random Vector Quantization (RVQ)

A large number of research contributions have been dedicated to the design of algorithms which categorize data into clusters or partitions according to some criteria. If codebook design is based on training set of data vectors, typically training set is clustered into 2^B clusters such that the minimum distance between the clusters is maximized. The Euclidean distance is used as the distance metric in the Lloyd's [40] and LBG algorithm [41]. Centers of the clusters form the 2^B-vector codebook. Lloyd's algorithm [40] is based on iterative clustering approach. First 2^B initial partition centers are defined and the whole set of data is partitioned based on minimum distance criteria, i.e., each vector in the data set belongs to the partition with the closest "center". In the next iteration the positions of the centers of the partitions are updated. The new center position is evaluated as an average over the vectors which belong to the partition. This iterative process continues until the partitions are stabilized. LBG algorithm [41] improves Lloyd's algorithm by better computation of the initial codebook.

The design of the codebook for feedback quantization and beamforming using Lloyd's algorithm has first been discussed in [42] which addresses MIMO feedback problem for point-to-point communications. It has been shown in [42] that the selection of the beamformers is based on maximizing the expected SNR which is equivalent to the vector quantization problem. Design of quantization codebooks

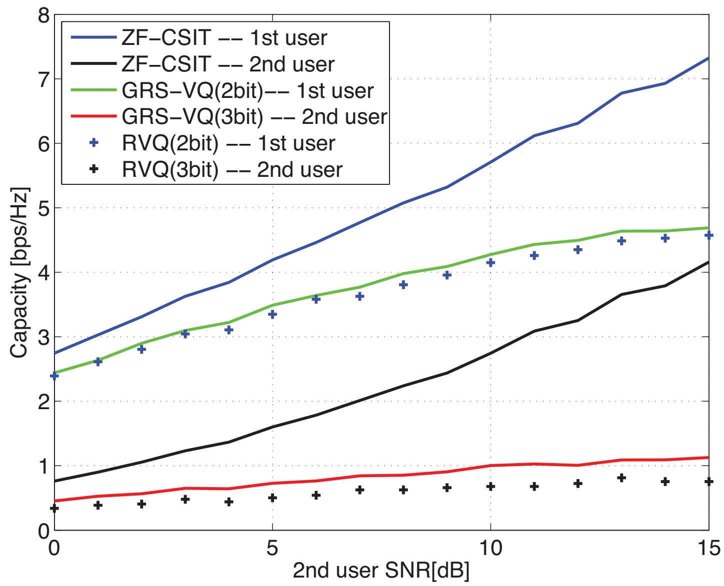

Figure 4.1: Capacity performance of Grassmannian and Random Vector Quantization with 2 and 3 feedback-bit.

based on LBG vector quantization is also widely used [41].

4.3.2 Grassmannian Line(Subspace) Packing

Grassmannian line packing is the problem of finding N lines ν_i, $i = 1, 2, \ldots, N$ passing through the origin in a M-dimensional space while maximizing the sine of the minimum angle between any two lines [43]. Codebook designed according to this criteria would be optimal to quantize channel vectors whose direction is uniformly distributed, see for example [35], deriving optimal beamforming vectors for i.i.d. MIMO Rayleigh flat-fading channels.

In Grassmannian line packing, the distance function between two lines is defined as [35]:

$$d\left(\nu_i, \nu_j\right) = \sin \Theta_{i,j} = \sqrt{1 - |\nu_i^{\dagger}, \nu_j|} \ .$$

Maximizing the minimum distance is equivalent to acquiring the smallest value for the magnitude correlation between any two vectors.

$$\delta\left(\mathbf{W}\right) = \min \sqrt{1 - |\nu_i^{\dagger}, \nu_j|^2} \ .$$

Sets of Grassmannian lines, $G(M, 2^B)$ can be used by single-antenna MS to quantize M-dimensional channel from a BS equipped with M antennas. In the case

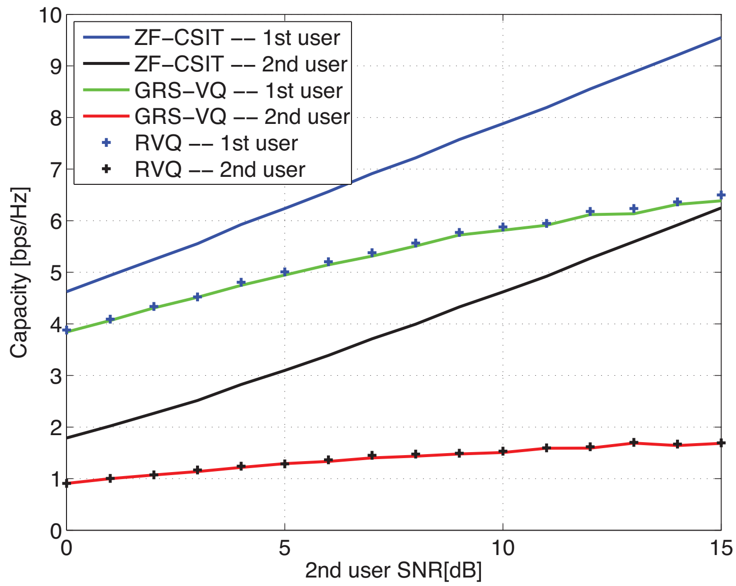

Figure 4.2: Capacity performance of Grassmannian and Random Vector Quantization with a large number of bits.

of a MS with $n > 1$ antennas, the problem of Grassmannian line packing is replaced by Grassmannian subspace packing, producing the set of subspaces $G(M, 2^B, n)$ [35]. Chordal distance is used as distance measure and is defined for two subspaces $\mathbf{F}_i$ and $\mathbf{F}_j$ as

$$d_{\text{chord}}(\mathbf{F}_i, \mathbf{F}_j) = \frac{1}{\sqrt{2}} ||\mathbf{F}_i {\mathbf{F}_i}^* - \mathbf{F}_j {\mathbf{F}_j}^*||_F \tag{4.9}$$

where F denotes the Frobenius norm. Grassmannian sets $G(M, N)$ and $G(N, N, n)$ are tabulated in [35,36,44]. Table 4.1 gives an example of a Grassmannian codebook which consists of $2^B = 8$ vectors and can be used for precoding at BS with $M = 3$ antennas requiring $B = 3$ bits of feedback.

4.4 Experimental Results

Downlink MIMO ZF beamforming with BS equipped with two antennas and two single-antenna MS has been modeled for various channel scenarios assuming perfect and quantized CSIT. For each channel realization, channel capacity based on SINR has been computed for each user and averaged over the channel realizations. In this work, the BS with $M = 2$ antennas beamforms to two users with a multiplexing

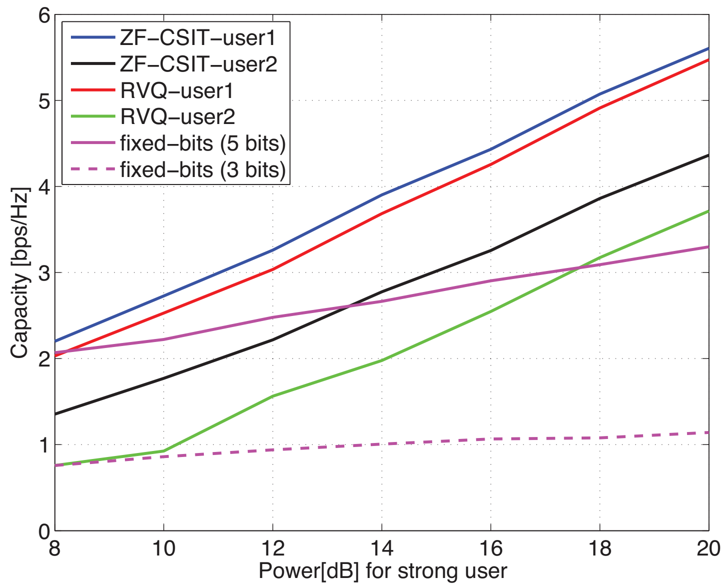

Figure 4.3: Capacity performance of Grassmannian and Random Vector Quantization with a constant number of feedback bits.

transmission scheme. The power allocation is applied before data transmission

$$\begin{bmatrix} y_1 \\ y_2 \end{bmatrix} = \mathbf{HG} \begin{bmatrix} P_{t_1} & 0 \\ 0 & P_{t_2} \end{bmatrix} \begin{bmatrix} d_1 \\ d_2 \end{bmatrix} + \begin{bmatrix} n_1 \\ n_2 \end{bmatrix}.$$

Fig. 4.1 displays the capacity performance for Rayleigh channel case where the transmit power allocated for the first user is 10dB higher than the power allocated for the second user. The results are plotted as a function of the 2nd user's SNR. Capacity for the 1st user (blue curve) and the 2nd user (black curve) assuming ideal CSIT are shown by the solid lines as well as capacity for the 1st user (green curve) and the 2nd user (red curve) assuming Grassmanian vector quantization with 2 and 3 feedback bits, respectively. Finally, the capacities of the 1st user (dotted blue) and 2nd user (dotted black) assuming random vector quantization with 2 and 3 feedback bits respectively, are also demonstrated. Note that this result is obtained from averaging the capacity performance of over 10000 channel coefficients. It can be observed that quantization with a fixed number of bits is not sufficient to maintain a fixed gap between quantized and ideal capacity performance. We can also notice that Grassmanian design outperforms RVQ for this case since Grassmanian vectors are optimal for the Rayleigh channel case.

Fig. 4.2 displays the capacity performance for the same setup as Fig. 4.1, however, a BS with 4 antennas is considered and each of two users has a single antenna.

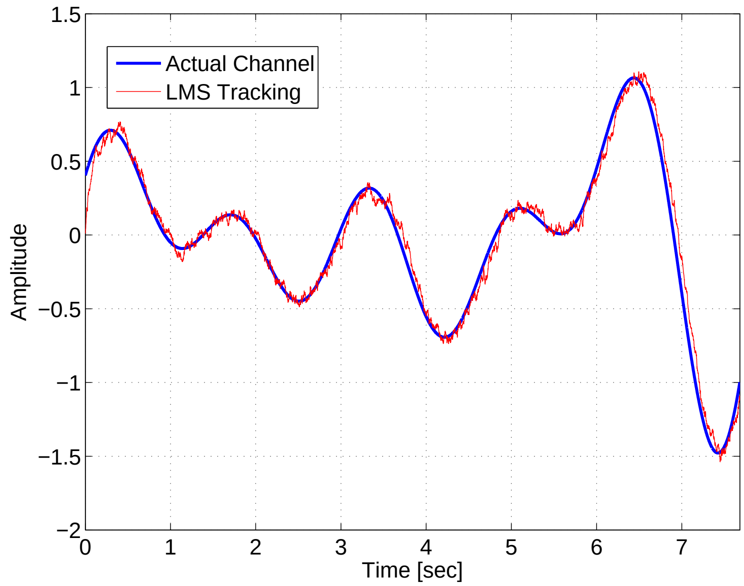

Figure 4.4: LMS channel tracking of the power of the wireless channel from the first BS antenna to the MS.

The results are plotted as a function of the 2nd user's SNR. Capacity for the 1st user (blue curve) and the 2nd user (black curve) assuming ideal CSIT are shown by the solid lines as well as capacity for the 1st user (green curve) and the 2nd user (red curve) assuming Grassmanian vector quantization with 7 and 8 feedback bits, respectively. Finally capacities of the 1st user (dotted blue) and 2nd user (dotted black) assuming random vector quantization with 7 and 8 feedback bits respectively is demonstrated. Despite the larger number of quantization bits used, the performance of the quantized system fails to grow at the same rate as with perfect CSIT. Grassmanian design outperforms RVQ, just as in the first experiment, but the difference is very small in this case.

Fig. 4.3 shows the capacity performance of the quantized system where the number of quantization bits scales with the user's SNR. Rayleigh channel case is selected for the simulation, averaging over 10000 channel coefficients, where the transmit power allocated for the first user (in dB) is twice the number of its quantization bits B_1 (on the X axis). The number of bits allocated to the second user $B_2 = B_1/2$ and its transmit power allocated for the first user (in dB) is twice the number of its quantization bits B_2. The capacity performance for the perfect CSIT case is shown by the blue (1st user) and black (2nd user) curves. The capacity performance for the RVQ case is shown by the green (1st user with B_1 bits) and red (2nd user with B_2

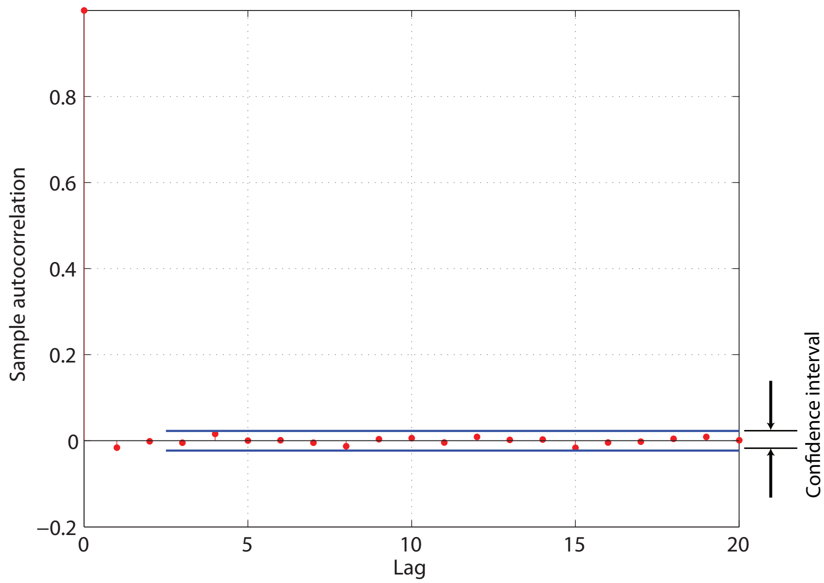

Figure 4.5: Autocorrelation function of the residual error.

bits) curves. Fig. 4.3 demonstrates that increasing the number of quantization bits linearly as a function of power (in dB) is sufficient to maintain a fixed distance to the optimal performance (see also (4.7)). The weaker user requires less quantization bits, as was pointed out by (4.8).

There are no confidence intervals shown in figures in this section. This is because the standard errors of the average capacity performances, based on sample sizes (i.e. the channel coefficients) of 10000, are in all cases no more than 0.9% of the reported averages. As such, error bars that correspond to even a 99.6% confidence interval (i.e. three standard errors to each side of the mean) are too small to be shown - the error bars are smaller than even the size of the symbols in the figures.

We are interested in analyzing the effect of different power transmission on the performance of the user's data, and how much feedback is required. Obviously, a user who receives the data with less power will suffer more in terms of SINR situation. Feeding back the CSI is more difficult for the former and we aim to ensure that this user is not required to send back large number of feedback bits to help the BS with beamforming (see Fig. 4.1 and Fig. 4.2).

4.4.1 Joint Channel Estimation and Quantization Feedback

In general, MIMO warless communication is sensitive to a large number of different factors such as quantization of CSI and its feedback, feedback delay, feedback error,

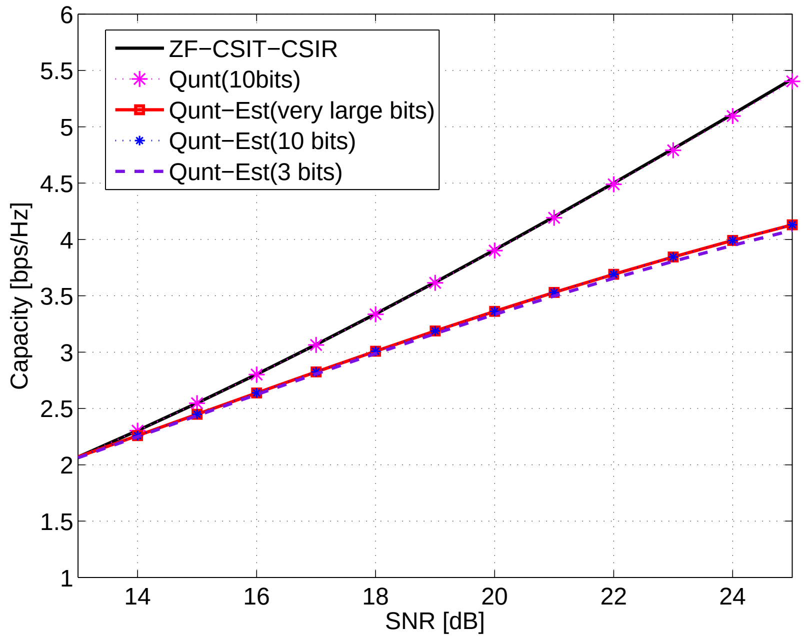

Figure 4.6: Capacity performance using different forms of CSIR and CSIT.

and obtaining receiver channel state information (CSIR). See [45] for a discussion of the above mentioned issues. Mathematical derivations of the previous subsections are performed for the case of perfect CSIR. Although channel estimation does not pose a major issue, perfect CSIR assumption is not realistic. In practice, not only quantization error, but the estimation error at the receiver influences system performance.

Fig. 4.4 demonstrates an example of the wireless channel tracking. Simulation setup includes the downlink MIMO channel where BS is employing two antennas and is communicating with a single antenna mobile. This wireless channel is generated by the SCM model with sampling rate of 1000Hz; see Section 2.4. The SNR of 10dB at the MS is considered. The tracking algorithm is the LMS algorithm with step-size $\mu = 0.05$; see Section 3. The step size's optimization in this simulation is based on minimizing the magnitude of the residual error which is reduced by approximately 12dB together with verifying the autocorrelation of the error (see Fig. 4.5). Note that the receiver must detect the transmitting vector from each antenna separately; this increases the level of interference at the MS. Considering our estimation performance in Fig. 4.4, the simulation in Fig. 4.6 is the ZF capacity performance of a downlink MU-MIMO scenario, having perfect and imperfect CSIR or CSIT knowledge. The

BS includes two antennas, multiplexing data to two users. This result indicates that when the estimation error is not negligible, the ZF capacity assuming perfect CSIT and CSIR (black curve) experiences performance degradation (red curve).

Assuming perfect CSIR, increasing the number of feedback bits leads to capacity growth (pink curve); see Section 4.2. However, with the non-negligible estimation error (imperfect CSIR), increasing the number of feedback bits does not change the capacity performance. It can be observed from Fig. 4.6 that 3-bit and 10-bit feedback quantization converge to same capacity as infinite number of feedback bits. A natural conclusion from the observed performance is that the number of quantization bits needs to be selected in correspondence of the channel estimation quality.

Chapter 5

Limited Feedback in Time-Varying Multipath MIMO Channels

In MIMO-multipath environments, communications system is considerably more vulnerable to multiuser interference in addition to inter-symbol interference (ISI) due to multipath effects. OFDM, a multicarrier modulation, is one of the transmission schemes which is an efficient way to deal with ISI. In Fig. 5.1, we can see a pictorial explanation of an OFDM block of data precoded by a cyclic prefix. In principle, the length of the prefix is long enough to avoid ISI. Duration of the OFDM symbol is much longer than the delay spread of the channel, which is the inverse of the coherence frequency separation. The delay spread of the channel is basically the difference between the time of arrival of the first component of the multipath and that of the last significant component. The concept of multicarrier modulation has been around for decades, and it has been standardized as the modulation scheme for the physical layer for many systems in the past few years (i.e., it is included in LTE air interference). As mentioned above, OFDM is a robust technique against frequency selective fading and intersymbol interference [46]; however, it can suffer from a high peak-to-average power ratio (PAPR) [47].

Another advantage of OFDM modulation is that it approaches the information theoretic capacity due to the water-filling power control across the multiple subcarriers. This leads to higher spectral efficiency of OFDM modulation scheme compared to wideband transmission approaches [48, 49]. The conventional concept of OFDM can further be extended to the field of MIMO. However, as discussed earlier in this thesis, MIMO in cellular networks is susceptible to multiuser interference, which

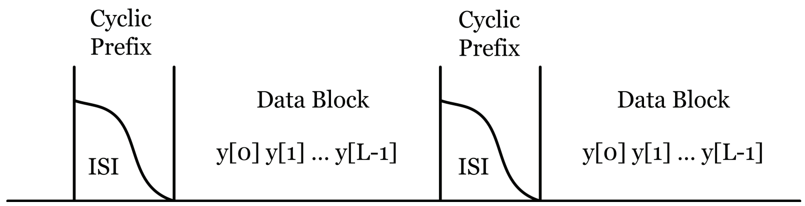

Figure 5.1: ISI in OFDM system.

can result from multiuser transmission techniques such as multiplexing on downlink transmission. This interference can reduce system performance significantly since serious SNR losses can be encountered. Different techniques are present in the literature for avoiding performance degradation due to interference. Typically data is precoded prior to downlink transmission such as zero-forcing precoding (section 2.2.2).

MIMO-OFDM technology and the frequency selectivity of MIMO channels are an important focus of LTE standardization; see Section 2.3. Thus, we study LTE downlink as it is the best candidate to exploit the MIMO multipath propagation.

5.1 Multipath Channel Model

A radio signal propagates from transmitter to receiver via distinct paths with different delays due to reflection, absorption, scattering and diffraction of the environmental objects. This creates a complex channel which is known as multipath channel, i.e., each path undergoes fading. Multipath signals experience random fluctuations during propagation. The term fading is referred to the random fluctuations of the amplitude. For non-line-of-sight (NLOS) environments, the received signal is modeled by

$$s(t) = \sum_{i=1}^{L} a_i \cos\left(w_c t + \phi_i\right),$$

L is the number of paths whose phase angles are distributed uniformly over $[0, 2\pi]$. The phase changes by 2π if the path length changes by one wavelength. However, if the transmitter and receiver move relative to each other, the effect of motion appears as a time-varying angle which results in a Doppler shift $f_d = \frac{f_c \nu}{c} \cos\psi_i$ [15], where f_c is carrier frequency and ν is the relative speed.

Often, the fading which is experienced in practice (i.e., small-scale fading) can be further classified into flat and frequency-selective fading. The signal is said to undergo flat fading if the received signal's spectral characteristics remain intact – or in other words, if the only effect is that the amplitude of the signal encounters variations. In this case, all frequency components of the signal are affected similarly by the channel, and the channel has a constant response over a bandwidth that is larger than that of the transmitted signal [50].

$$B_s \ll B_c$$

$$\tau_s \gg \tau_c$$

This occurs when the delays of the different signal paths are shorter than the coherence time τ_c of the channel, which is typically of the order of a few ms. Similarly, if the delays exceed the coherence time, different frequency components of the signal will undergo different fadings.

5.1.1 LTE Multipath Characteristics

The SCM model generates multipath channels in representative urban and suburban scenarios. As was discussed earlier, the characteristics of the multipath is defined by the time delay spread of the channel. In wireless communications, the delay spread results in frequency-selectivity of the channel (i.e., ISI) if the duration of the symbol time traveling is smaller than the time delay spread of the channel. Signal propagation in a mobile environment can be modeled by the multipath model [51]. Therefore, the impulse response of the wide-sense stationary uniform scattering (WSSUS) (where the taps are statistically independent) fading channel is represented by [52]

$$w(\tau, t) = \sum_{\ell=0}^{L-1} w_\ell(t)\delta(\tau - \tau_\ell).$$

As mentioned earlier, the SCM is used to generate LTE and high-speed downlink packet access (HSDPA) channel models. HSDPA transmission is a high data rate transmission standard with a symbol-time interval of 0.26μsec which is exposed to ISI and multipath effects. Fig. 5.2 shows the delay spread of the system which, is at least 10 times larger than the HSDPA transmission symbol rate. In this histogram, we include all paths which have 0.1% energy of the path with maximum energy.

However, on LTE downlink, the data transmission rate of 71μsec results in smaller delay spread compared to the symbol-time interval; see Fig. 5.2. The de-

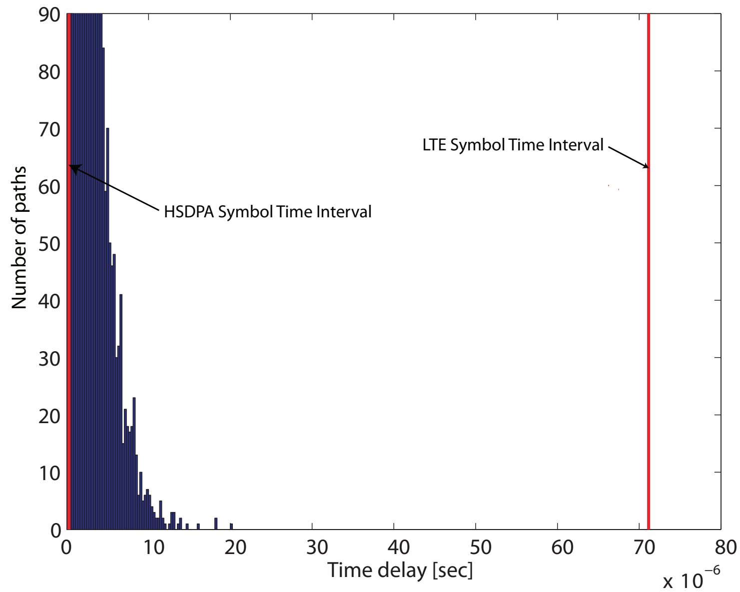

Figure 5.2: Multipath delay spread histogram in the macro urban scenario.

lay spread is approximately $\tau_c = 18$ μsec with $\tau_{\text{HSDPA}} \ll \tau_c \ll \tau_{\text{LTE}}$. The symbol duration time for HSDPA and LTE are also shown by vertical lines in Fig. 5.2.

Fig. 5.3 illustrates the frequency response of the HSDPA channel in the presence of multipath. As can be seen, the signal undergoes several cycles of fading. Note that the number of distinct paths are 6, which is the maximum number of paths that SCM model supports. The frequency response of LTE multipath channel is also depicted in Fig. 5.4. It can be seen that the frequency components of the LTE downlink experience similar variations, which is known as flat fading; see Section 5.1.

In practice, distinct paths are received by the user with different delays. However, the delays are not a function of the OFDM symbol-time interval. The receiver should acquire the discrete-time information of the multipath for further processes (see 5.1).

5.2 Channel Estimation in MIMO-OFDM

Channel estimation is a well-investigated subject in single-carrier wireless communication systems; see Chapter 3. The most typical approach in estimating the channel is to allocate pilot sequences in the data transmission frame. Pilots are known by both the transmitter and the receiver. This approach has low computational complexity and is relatively robust [53]. However, pilots carry no information and are intrinsically wasteful in bandwidth. Pilot allocation is done in different ways in an

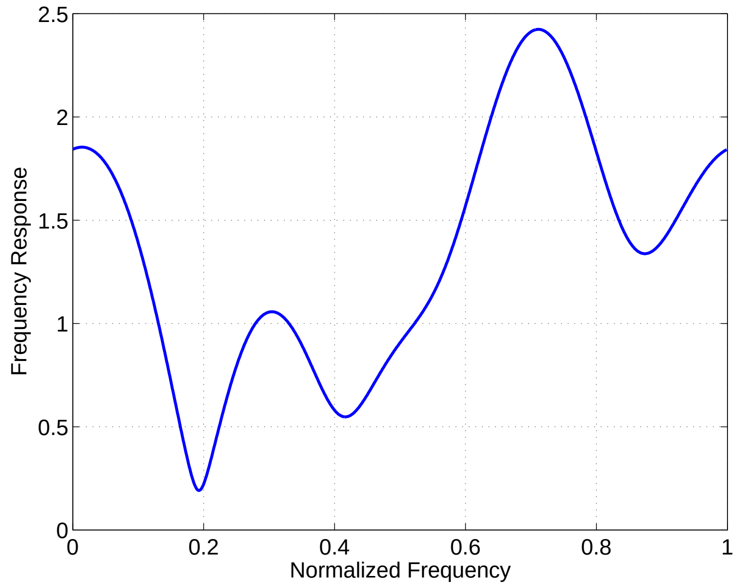

Figure 5.3: Frequency response of the multipath in macro urban scenario-HSDP.

OFDM system, i.e., block-type pilot subcarrier arrangement and combo-type pilot sub-carrier arrangement [54].

In pilot-based estimation, a larger number of transmit antennas require longer pilot sequences, which is not agreeable to wireless communications. One approach to avoid long pilot sequences is to use the semi-blind channel estimators, meaning that the transmitted data assists the pilots for the sake of channel estimation [55, 56].

5.2.1 Channel Estimation in LTE

To date, not much study has been devoted to the specific ways of estimating channel in standardized systems such as LTE. Recently, researchers have attempted to design feasible algorithms for channel estimation in LTE, while accounting for simplicity and reliability [52, 57–59]. In MIMO-OFDM, channel estimation highly depends on the variation and time-frequency selectivity of the channel. Pilots are the best candidates to counteract channel variations. An applied interpolation over the collected channel samples from the pilots makes channel prediction feasible in highly dynamic environments. Pilots in LTE are allocated according to the identity matrix with elements $\sqrt{\rho}\exp(i\theta)$. In the case of white Gaussian noise, the pilot allocation is optimal in terms of minimizing the variance of an estimation error [60].

LTE resource blocks are equipped with pilots which are placed in specific and standardized locations on each subcarrier [61]; see Fig. 5.5. Pilots are embedded in

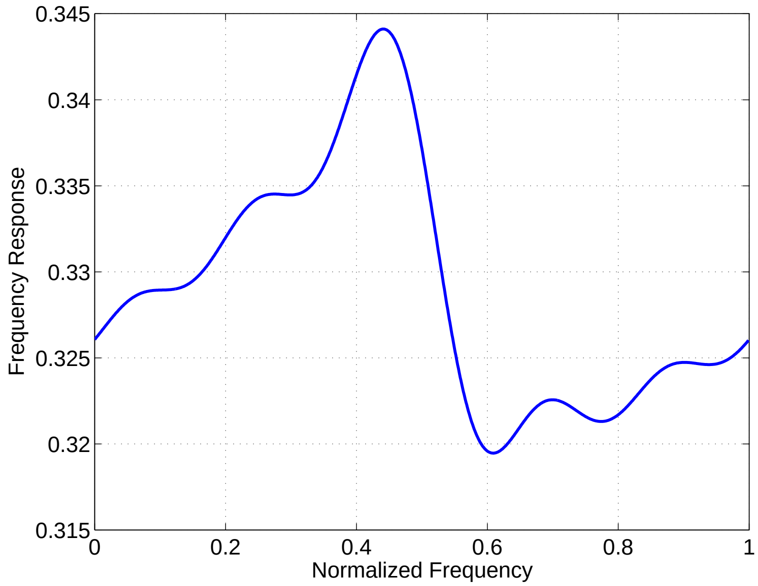

Figure 5.4: Frequency response of the multipath in macro urban scenario-LTE.

the orthogonal time-frequency grids and are known as scattered pilots. However, these pilots are redundant as they are sent too frequently for many channel realizations. In short, pilots do not carry new information if they are transmitted too frequently over the channel [51, 62]. Therefore, it is good practice to estimate how frequently the channel changes for typical user speeds and channel models. Often, the transmitted signal with a certain carrier frequency f_c is received as a shifted frequency $f_c \pm f_d$. This shift results from mobility of the channel and is known as the Doppler frequency.

5.2.2 OFDM Structure in Terms of Estimation

OFDM is a multicarrier technique which adds a new dimension to the single carrier estimation approach; see Chapter 5. It is a common practice to assume the channel to be constant over an OFDM symbol duration [63]. Estimation in OFDM can be considered a 2-dimensional process. Every OFDM symbol has a location on a time-frequency grid which needs to be tracked in both dimensions.

In OFDM, subcarriers undergo different fadings depending on the delay spread or coherence frequency. Therefore, the frequency spacing has to be adjusted carefully and the Nyquist sampling theorem should be applied in the frequency domain to specify the subcarrier spacing [64].

$$D_p \leq \frac{1}{\tau_{\max} \Delta df}$$

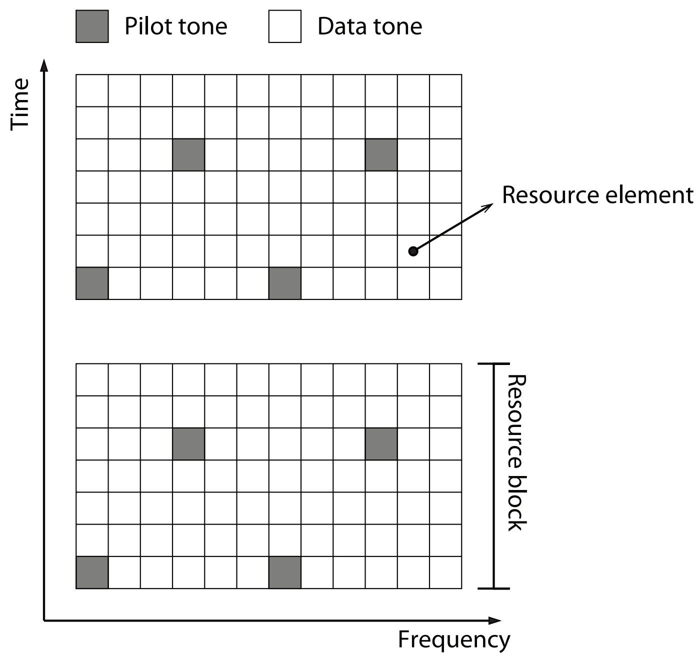

Figure 5.5: LTE time-frequency resource grid with pilot locations.

In situations where the channel is changing across the OFDM symbols, pilot tones are required to be inserted at appropriate spacing, which is a function of the coherence time and Doppler spread. The maximum spacing of the pilot tone is given by

$$D_t \leq \frac{1}{2 f_{d_{\max}} T_f}$$

where $f_{d_{\max}}$ is the maximum Doppler spread and T_f is the OFDM symbol duration. The pilot patterns are vital to the system. Transmit power and spectral efficiency on the one hand, and estimation accuracy on the other hand, strongly depend on the pilot pattern in an OFDM system. One of the main approaches in this trade-off process is the exploitation of subcarrier correlation [65]. Often, the subcarriers at both ends of an OFDM symbol are highly correlated; this characteristic can be used for precise channel estimation. Therefore, the challenge is to find the optimum pilot locations to provide the receiver with the best estimate of time and frequency aspects of the channel. However, pilot allocation varies with the Doppler spread of the channel and usually needs to be designed locally; it must also satisfy the Nyquist rate of the respective channel. Further, adaptive pilot allocation is introduced to improve the performance in terms of estimation accuracy and overhead avoidance [66].

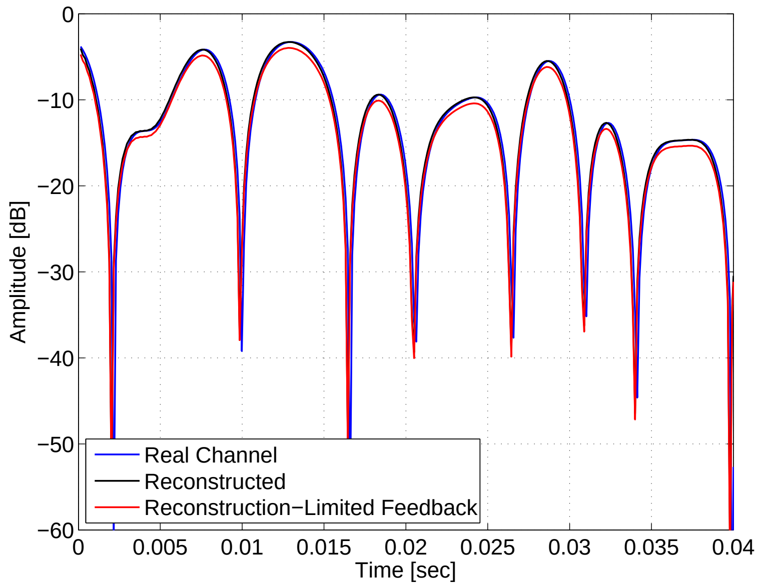

Figure 5.6: SCM signal Reconstruction with Doppler rate and 8-bit feedback per sample.

5.3 LTE Channel Reconstruction at Transmitter

The Nyquist theorem ensures the exact reconstruction of the continuous channel function. However, the frequency of the feedback transmission is crucial to the channel reconstruction at the transmitter due to the restrictions of feedback quantization. Based on the Nyquist-Shannon sampling theorem, the Nyquist rate of the channel is given by $T_{\text{Nyquist}} = 2B_{\text{channel}}$, where the channel bandwidth is proportional to the sampling frequency by the amount of frequency components which carry $1/\sqrt{2}$ of the maximum power frequency component [10].

The process of signal reconstruction can be done by a simple interpolation process, or low pass filtering of the signal with impulse response of $\text{sinc}(t/T)$. If the Doppler spread is larger than the Nyquist rate, the sampling theorem would not apply. The linear interpolation is given by [67]

$$y(t) = \sum_{n=-\infty}^{\infty} x(nT)\,\text{sinc}(\frac{n}{T} - n) \tag{5.1}$$

Fig. 5.6 and Fig. 5.7 depict channel reconstructions of the SCM environment.In this MIMO multipath simulation set up with two transmit antennas and six paths (see Fig. 5.6), the user velocity is 100km/h, the feedback rate is $v/(2\lambda)$, which is approximately 19 times smaller than the data transmission rate. As can be seen from Fig. 5.6 and Fig. 5.7, the signal-of-interest undergoes fading through time.

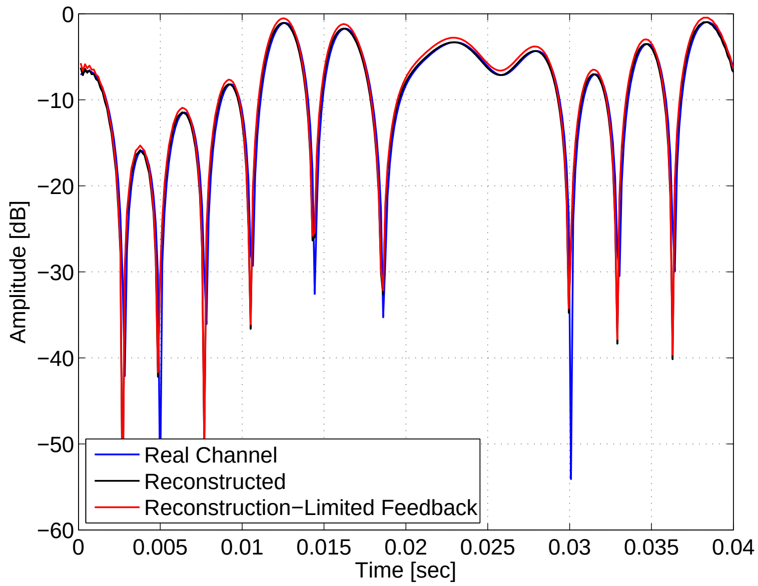

Figure 5.7: SCM signal Reconstruction sampled at 4 times Doppler rate with 2 bits of feedback per sample.

In the SCM environment, the transmission rate is defined as $\lambda/(2vD_s)$, where the sampling density D_s is the number of samples per half wavelength. The performance characteristics of this simulation are tabulated in Table 5.1. The time variation of a multipath channel is defined by its Doppler spread. In other words, the Doppler spread is the combined Doppler shift of all paths with different angles of arrival. The coherence time of the channel is inversely proportional to the Doppler spread of the channel, i.e., $\tau_c = 1/D_s$.

It can be observed from our results in Table 5.1 that signal reconstruction is more efficient if it occurs less frequently with larger feedback bits. This is also more agreeable to practice, since it reduces traffic on the uplink channel.

5.4 Feedback Schemes for Multipath MIMO Channels with LTE

In frequency division duplexing systems, CSIT is not provided by channel reciprocity and explicit closed-loop feedback is required. In practice, this information is transmitted in quantized form and is sent as overhead on the uplink channel, enabling the transmitter to utilize it, for example, for beamforming; see Section 4.2.

The basic feedback scheme in MIMO-OFDM systems is to report the channel of each subcarrier back to the transmitter. Assuming 512 subcarriers, this would

Table 5.1: SCM signal reconstruction comparison at the transmitter.

Feedback Rate	Sampling Time	# of Bits	Recons Error [dB]	Feedback Recons Error [dB]
F_d	$\approx 19 \times T_d$	8	-22.14	-17.03
$4 \times F_d$	$\approx 4 \times T_d$	2	-22.15	-3.58

result in a large amount of information and can lead to channel overload; it is basically redundant due to the high correlation of subcarriers. Another possible approach is to feed back the channel information in the time domain, which reduces much redundancy in the uplink transmission; see Fig. 5.8. However, unlike in SISO systems, a small amount of feedback is not sufficient to achieve the MIMO capacity. In addition, in the multipath environment, some of the paths carry more power than others and need to be quantized accordingly; one such approach, for example, utilizes the distortion rate method [45].

The LTE Channel

Applying the Fourier transform over the transmission and reception is a linear process of low complexity. The Fourier transform can be effectively applied to the transmission process of the system and diagonalize the channel matrix [68],

$$\mathbf{y}^{(F)} = \mathbf{F}\mathbf{H}_{\text{ISI}}\mathbf{F}^{H}\mathbf{x}^{(F)} + \mathbf{F}\eta \tag{5.2}$$

N_c is the number of subcarriers and $\mathbf{F}$ is the Fourier matrix which translates the channel into the frequency domain. The enteries of the Fourier matrix are

$$\mathbf{F}(k,n) = \mathbf{e}^{-j\frac{2\pi kn}{N_c}}$$

which are elements of a unitary $N_c \times N_c$ matrix when normalized by $\sqrt{N_c}$, and therefore the inverse Fourier transform or IDFT matrix is $\mathbf{F}^{-1} = \mathbf{F}^{H}$. Also, $\mathbf{H}_{\text{ISI}}$ in (5.2) is a circulant convolution matrix and involves cyclic prefix (CP) which is required for OFDM transmission.

$$\mathbf{H}_{\text{ISI}} = \begin{bmatrix} h_0 & h_1 & \cdots & h_L & & & \\ & h_0 & h_1 & \cdots & h_L & & \\ & & \ddots & \ddots & \ddots & \ddots & \\ & & & h_0 & h_1 & \cdots & h_L \\ & & & & \ddots & \ddots & \vdots \\ h_2 & \cdots & h_L & & & h_0 & h_1 \\ h_1 & h_2 & \cdots & h_L & & & h_0 \end{bmatrix}_{N_c \times N_c}$$

The channel Fourier operation (5.2) can be further simplified to

$$y^{(F)} = \mathbf{D}\mathbf{x}^{(F)} + \mathbf{F}\eta$$

where $\mathbf{D}$ is a diagonal matrix in a SISO system and a block matrix of diagonal submatrices in MIMO systems where each relates to a transmitter-receiver channel in the multi-antenna system (see (5.3)).

$$\mathbf{H}_{\text{MIMO-ISI}} = \begin{bmatrix} \mathbf{H}_{\text{ISI}}^{0,0} & \cdots & \mathbf{H}_{\text{ISI}}^{0,M-1} \\ \vdots & \ddots & \vdots \\ \mathbf{H}_{\text{ISI}}^{N-1,0} & \cdots & \mathbf{H}_{\text{ISI}}^{N-1,M-1} \end{bmatrix}_{N\times M} \tag{5.3}$$

Therefore, to apply ZF beamforming in transmission scheme for LTE system, the precoding matrix is

$$\mathbf{D}^{-1} = \mathbf{F}\mathbf{H}_{\text{ISI}}{}^{-1}\mathbf{F}^{H}.$$

The system we analyze in this section includes a BS with $M = 2$ antennas and $K = M$ single-antenna users. The users are placed close to each other on the cell edge and no user cooperation is assumed. The BS uses orthogonal subcarriers to multiplex data to both users of interest. The inverse of the effective channel is applied as precoding matrix to zero-force data transmission. The capacity of the MIMO-OFDM system is given by [69]

$$C_{\text{sum}} = \frac{1}{N_c} \log\left[\det\left(\mathbf{I}_{N_c} + \frac{\rho}{M}\mathbf{H}\mathbf{H}^{\dagger}\right)\right]$$

where ρ is the SNR at the receiver side.

We assume perfect knowledge of the channel at the receiver which can be provided by the pilots embedded in each subcarrier; see Section 5.2. In Fig. 5.8, a similar scenario to that in Section 4.4 is considered. The communications system is an LTE channel model with 2 transmit antennas at the BS serving two users. The users are assumed to differ in SINR condition, with the stronger user having 12dB higher SINR. Note that the ZF capacity performance of the stronger user is of interest, and the weaker user will act as an interference; see (4.3). In this experiment, an approximately equal number of bits in both the time domain and the frequency domain has been considered for a fair comparison. It has been shown previously that, as the transmit power grows, the number of feedback bits should increase to maintain the required capacity performance (see (4.7)). For example, for 15dB of SNR, both the time and frequency domain approaches result in approximately 2

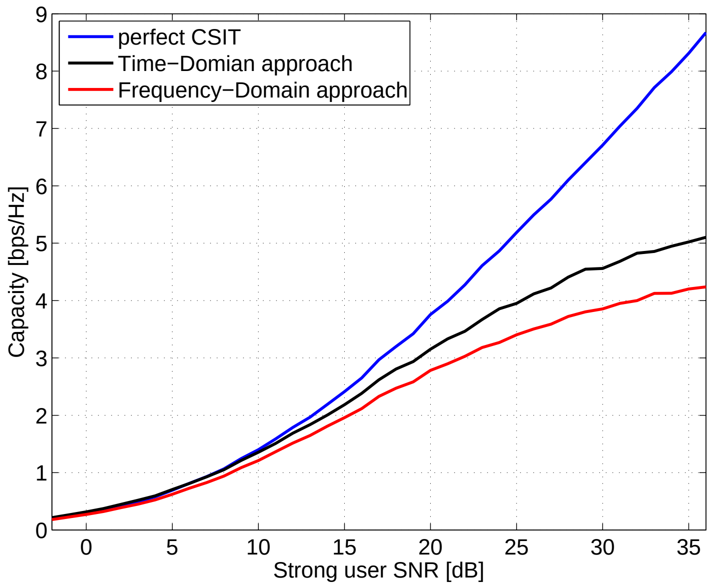

Figure 5.8: ZF capacity performance for LTE.

bits/sec/Hz capacity; see Fig. 5.8. An exact approach in frequency domain is exploiting the channel knowledge via the correlation of the subcarriers and applying interpolation. However, the correlation in frequency domain is not a priori known and finding about the exact interpolation is not straightforward. Therefore, the interpolation itself and in particular, the number of feedback quantization required for a correct value of subcarrier interpret complexity. However, in principle, the approach in frequency domain should result in similar ZF performance as in time domain. In Fig. 5.8, 5000 SCM coefficient channels is used to obtain the average capacity; to smooth the performance, larger number of channel coefficients is needed. 5×8 bits in time domain and 16×3 bits of feedback in frequency domain is applied for downlink precoding. The simple averaging interpolation is used in frequency domain approach to reduce the number of feedback bits transmission. Evidently, the feedback in time domain approach is much more efficient than that of frequency domain and results in better performance. This result is compatible with practice since the uplink traffic in time domain approach is avoided.

Chapter 6

Concluding Remarks and Future Work

The main contribution of this MSc thesis is the extension to the prior work on feedback quantization for flat channels [32] to realistic wireless channels typical for cellular telecommunication. Spatial Channel Model (SCM) is used to generate practical channels. In addition, we consider transmission characteristics of the practical communications system standards, i.e., LTE. The relationship between the number of feedback bits and transmit power is analyzed for the case of different SINR levels of the mobile users. The analytical and experimental results show that a stronger user requires more feedback bits to maintain the same gap to capacity as the weaker user. The second contribution is a study of feedback quantization in the presence of imperfect CSIR. The channel is estimated at the mobile stations using LMS algorithm. The effect of non-negligible estimation error on ZF downlink precoding performance has been considered. Our results suggest that the use of larger codebook cannot compensate for performance degradation due to estimation error.

The third contribution is a study of feedback quantization for multipath channels and LTE downlink transmission. For the case of multipath environment, this study shows that the time domain quantization and feedback is more practical and efficient than frequency domain quantization and feedback. As the subcarrier correlation is not known a priori to the feedback quantization, subcarrier interpolation results in losses which can be avoided if quantization is performed in the time domain for each path. Finally, the fourth contribution demonstrates that the frequency of feedback transmission should be based on the mobility of the channel – not the frequency of the pilot transmission. Pilot transmission is more frequent for a reliable estimation of the channel in LTE. The frequency of feedback transmission, however, should be avoided if the channel remains unchanged.

In this regard, Chapter 2 discusses the MIMO techniques for cellular networks and interference avoidance in multiuser communications. Next, the characteristics of the LTE system are reviewed and the Spatial Channel Model is introduced as a realistic channel generator for this study. Chapter 3 examines the use of adaptive filters and the family of steepest-descent algorithms. Further investigations are then carried out by exploiting the reliability of simple and practical channel estimation techniques - the LMS algorithm. This is to acquire channel knowledge at the receiver with minimal error.

Chapter 4 addresses the acquiring of channel information at the transmitter. For that purpose, the ZF capacity at the receiver is used as a metric for system performance. Imperfect channel information is processed in terms of (a) the number of feedback bits and the accuracy of the feedback scheme, and (b) codebook design in more practical environments, such as different SINR situations for the users. The consistency of the number of feedbacks, with SNR condition of the users, is analyzed and discussed in detail. Next, the inherent complications with LTE system are discussed in regard to the MIMO-OFDM transmission technique within the LTE standard. The high transmission data rate and high mobility of the channel environment in LTE system can exacerbate the degrading effect of imperfect channel information.

Chapter 5 therefore focuses the research on this aspect and analyzes the ZF performance in both frequency and time domain. It is shown from this analysis that time-domain quantization feedback is far more efficient in terms of performance and uplink overload.

Although we have studied channel estimation performance using the LMS algorithm, more complex adaptive algorithms, such as RLS algorithm and Kalman filters, are also reliable candidates for performance improvement. Channel prediction due to data aging further adds new challenges to the estimation process, especially in very mobile environments. Zero-forcing is only one of the several precoding techniques for avoiding interference and maximizing throughput in receiver antenna systems. Other precoding techniques are also of interest.

For various multipath profiles, algorithms can be designed to compress quantization feedback for error optimization. Caire *et al.* [70], for example, has proposed the application of rate distortion for time-domain limited feedback. It is likely that, in the near future, suboptimal quantization feedback algorithms will be a topic of intense research interest.

Adaptive transmit antenna techniques, user selection and opportunistic signaling will assure system capacity enhancement with the growth of the number of users in the system. However, this requires exact knowledge of the channel. Therefore, enriching the techniques of acquiring exact channel knowledge will enable the system to utilize such techniques to assure capacity growth.

Bibliography

[1] G. T. 25.996, "Spatial channel model for multiple input multiple output (MIMO) simulations (Release 6)." 2003.

[2] A. T. Harri Holma, *WCDMA For UMTS: HSPA Evolution And LTE,*. New York: John Wiley & Sons, 2009.

[3] A. J. Paulraj, D. A. Gore, R. U. Nabar, and H. Bölcskei, "An overview of MIMO communications - a key to gigabit wireless," *Proc. IEEE*, vol. 92, pp. 198–218, Feb. 2004.

[4] D. Gesbert, H. Bölcskei, D. Gore, and A. Paulraj, "MIMO wireless channels: capacity and performance prediction," in *Global Telecommunications Conference, 2000. GLOBECOM '00. IEEE*, vol. 2, San Francisco, CA, Aug. 2002, pp. 1083–1088.

[5] V. Tarokh, N. Seshadri, and A. R. Calderbank, "Space-time codes for high data rate wireless communication: performance criterion and code construction," *IEEE Trans. Inf. Theory*, vol. 44, no. 2, pp. 744–765, Mar. 1998.

[6] S. M. Alamouti, "A simple transmit diversity technique for wireless communications," *IEEE J. Sel. Areas Commun.*, vol. 16, no. 8, pp. 1451–1458, 1998.

[7] N. K. Das, T. Inoue, T. Taniguchi, and Y. Karasawa, "An experiment on MIMO system having three orthogonal polarization diversity branches in multipath-rich environment," in *Vehicular Technology Conference, 2004. VTC2004-Fall. 2004 IEEE 60th*, vol. 2, 2004, pp. 1528–1532.

[8] F. G. J., "Layered space-time architecture for wireless communication,," *Bell Labs Technical Journal*, vol. 1, pp. 41–59, 1996.

[9] A. J. Paulraj and T. Kaillath, "Increasing capacity in wireless broadcast systems using distributed transmission/directional reception,," *Bell Labs Technical Journal*, 1994.

[10] C. E. Shannon, "The mathematical theory of communication,," *Bell Syst, Tech J.*, vol. 27, no. 2, pp. 379–423, 1948.

[11] C. C. Martin, J. H. Winters, and N. R. Sollenberger, "Multiple-input multiple-output (MIMO) radio channel measurements," in *Antennas and Propagation Society International Symposium, 2001. IEEE*, vol. 1, Boston, MA, Jul. 2001, pp. 418–421.

[12] J. Ling, D. Chizhik, P. Wolniansky, R. Valenzuela, N. Costa, and K. Huber, "Multiple transmit multiple receive (MTMR) capacity survey in manhattan," *Electronics Letters*, vol. 37, no. 16, pp. 1041–1042, Aug. 2001.

[13] R. M. Buehrer, S. Arunachalam, K. H. Wu, and A. Tonello, "Spatial channel model and measurements for IMT-2000 systems," in *Vehicular Technology Conference, 2001. VTC 2001 Spring. IEEE VTS 53rd*, vol. 1, Rhodes, May 2001, pp. 342–346.

[14] D. Astely, E. Dahlman, A. Furuskar, Y. Jading, M. Lindstrom, and S. Parkvall, "LTE: the evolution of mobile broadband," *IEEE Commun. Mag.*, vol. 47, pp. 44–51, Apr. 2009.

[15] P. V. David Tse, *Fundamentals of Wireless Communications,*. New York: Cambridge Press University, 2005.

[16] G. J. Foschini and M. J. Gans, "On limits of wireless communications in a fading environment when using multiple antennas," *Wirel. Pers. Commun.*, vol. 6, no. 3, pp. 311–335, 1998.

[17] E. Telatar, "Capacity of multi-antenna Gaussian channels," *European Transactions on Telecommunications*, vol. 10, no. 6, pp. 585–596, 1999.

[18] S. Maruyama, S. Ogawa, and K. Chiba, "Mobile terminals toward LTE and requirements on device technologies," in *VLSI Circuits, 2007 IEEE Symposium on*, Kyoto, Jun. 2007, pp. 2–5.

[19] Zyren, "Overview of the 3gpp long term evolution physical layer,," Dr. Wes McCoy, Tech. Rep., 2007.

[20] E. Damosso and L. M. Carreia, "Cost 231 final report," http://www.gsmworld.com/, 1999.

[21] S. Haykin, *Adaptive Filter Theory*, 2nd ed. Prentice Hall, 1991.

[22] H. Zhu, B. Farhang-Boroujeny, and C. Schlegel, "Pilot embedding for joint channel estimation and data detection in MIMO communication systems," *IEEE Commun. Lett.*, vol. 7, pp. 30–32, Jan. 2003.

[23] B. Farhang-Boroujeny, "Pilot-based channel identification: proposal for semi-blind identification of communication channels," *Electronics Letters*, vol. 31, pp. 1044–1046, Jun. 1995.

[24] C. K. Ho, B. Farhang-Boroujeny, and F. Chin, "Added pilot semi-blind channel estimation scheme for OFDM in fading channels," in *Global Telecommunications Conference, 2001. GLOBECOM '01. IEEE*, vol. 5, San Antonio, TX, Nov. 2001, pp. 3075–3079.

[25] J. K. Cavers, "An analysis of pilot symbol assisted 16QAM for digital mobile communications," in *Vehicular Technology Conference, 1991. Gateway to the Future Technology in Motion., 41st IEEE*, St. Louis, MO , USA, Nov. 1991, pp. 380–385.

[26] C. E. Shannon, "The zero error capacity of a noisy channel," *IRE Trans. Inform. Theory*, Sep. 1956.

[27] F. Floren, O. Edfors, and B. A. Molin, "The effect of feedback quantization on the throughput of a multiuser diversity scheme," in *Global Telecommunications Conference, 2003. GLOBECOM '03. IEEE*, vol. 1, Dec. 2003, pp. 497–501.

[28] T. Tang and R. W. Heath, "Opportunistic feedback for downlink multiuser diversity," *IEEE Commun. Lett.*, vol. 9, no. 10, pp. 948–950, Oct. 2005.

[29] P. Viswanath, D. N. C. Tse, and R. Laroia, "Opportunistic beamforming using dumb antennas," in *Information Theory, 2002. Proceedings. 2002 IEEE International Symposium on*, Jun. 2002.

[30] T. Yoo, N. Jindal, and A. Goldsmith, "Multi-antenna downlink channels with limited feedback and user selection," *IEEE J. Sel. Areas Commun.*, vol. 25, no. 7, pp. 1478–1491, Sep. 2007.

[31] N. Chiurtu, B. Rimoldi, and E. Telatar, "On the capacity of multi-antenna gaussian channels," in *Information Theory, 2001. Proceedings. 2001 IEEE International Symposium on*, Washington, DC, Jun. 2001.

[32] N. Jindal, "MIMO broadcast channels with finite-rate feedback," *IEEE Trans. Inf. Theory*, vol. 52, no. 11, pp. 5045–5060, Nov. 2006.

[33] D. J. Love, J. Heath, R. W., W. Santipach, and M. L. Honig, "What is the value of limited feedback for MIMO channels?" *IEEE Commun. Mag.*, vol. 42, no. 10, pp. 54–59, Oct. 2004.

[34] D. J. Love, R. W. Heath, V. K. N. Lau, D. Gesbert, B. D. Rao, and M. Andrews, "An overview of limited feedback in wireless communication systems," *IEEE J. Sel. Areas Commun.*, vol. 26, no. 8, pp. 1341–1365, Oct. 2008.

[35] D. J. Love, J. Heath, R. W., and T. Strohmer, "Grassmannian beamforming for multiple-input multiple-output wireless systems," *IEEE Trans. Inf. Theory*, vol. 49, no. 10, pp. 2735–2747, Oct. 2003.

[36] C. Simon and G. Leus, "Feedback quantization for linear precoded spatial multiplexing," *EURASIP J. Adv. Signal Process*, vol. 2008, pp. 1–13, 2008.

[37] W. Santipach, "Tree-structured random vector quantization for beamforming in a multiantenna channel," in *Electrical Engineering/Electronics, Computer, Telecommunications and Information Technology, 2008. ECTI-CON 2008. 5th International Conference on*, vol. 1, Krabi, 2008, pp. 325–328.

[38] R. Samanta and R. W. Heath, "Codebook adaptation for quantized MIMO beamforming systems," in *Signals, Systems and Computers, 2005. Conference Record of the Thirty-Ninth Asilomar Conference on*, Pacific Grove, CA, Oct. 2005, pp. 376–380.

[39] V. Raghavan, R. W. Heath, and A. V. Sayeed M., "Systematic codebook designs for quantized beamforming in correlated MIMO channels," *IEEE J. Sel. Areas Commun.*, vol. 25, no. 7, pp. 1298–1310, Sep. 2007.

[40] A. Gersho and R. M. Gray, *Vector Quantization and Signal Compression.* Boston: Kluwer,, 1992.

[41] Y. Linde, A. Buzo, and R. Gray, "An algorithm for vector quantizer design," *IEEE Trans. Commun.*, vol. 28, no. 1, pp. 84–95, Jan. 1980.

[42] A. Narula, M. J. Lopez, M. D. Trott, and G. W. Wornell, "Efficient use of side information in multiple-antenna data transmission over fading channels," *IEEE J. Sel. Areas Commun.*, vol. 16, no. 8, pp. 1423–1436, Oct. 1998.

[43] J. H. Conway, R. H. Hardin, and N. J. A. Sloane, "Packing lines, planes, etc.: Packings in grassmannian spaces," *Exper. Math.*, vol. 5, no. 2, pp. 139–159, 1996.

[44] N. J. A. Sloane, "Packings in grassmannian spaces," http://www.research.att.com/∼njas/grass/.

[45] G. Caire, N. Jindal, M. Kobayashi, and N. Ravindran, "Multiuser MIMO achievable rates with downlink training and channel state feedback," *IEEE Trans. Inf. Theory*, vol. 56, no. 6, pp. 2845–2866, May 2009.

[46] A. Bahai and B. Saltzberg, *Multi-Carrier Digital Communications, Theory and Application of OFDM.* Kluwer Academics, 2002.

[47] S. H. Han and J. H. Lee, "An overview of peak-to-average power ratio reduction techniques for multicarrier transmission," *IEEE Trans. Wireless Commun.*, vol. 12, pp. 56–65, Apr. 2005.

[48] S. Kasturia and J. M. Aslanis, J. T. Cioffi, "Vector coding for partial response channels," *IEEE Trans. Inf. Theory*, vol. 36, pp. 741–762, Jul. 1990.

[49] J. M. Cioffi, "Digital communications, chapter 4: Multichannel modulation," Unpublished course notes.

[50] A. Goldsmith, *Wireless Communications*. New York: Cambridge Press University, 2005.

[51] 3rd Generation Partnership Project, "Technical specification group radio access netwroks; deployment aspects,," Tech. Rep. 7, June 2007.

[52] L. A. M. Ruiz de Temino, C. Navarro i Manchon, C. Rom, T. B. Sorensen, and P. Mogensen, "Iterative channel estimation with robust wiener filtering in LTE downlink," in *Vehicular Technology Conference, 2008. VTC 2008-Fall. IEEE 68th*, Calgary, BC, 2008, pp. 1–5.

[53] Y. Zhao and A. Huang, "A novel channel estimation method for OFDM mobile communication systems based on pilot signals and transform-domain processing," in *Vehicular Technology Conference, 1997 IEEE 47th*, vol. 3, Phoenix, AZ, 1997, pp. 2089–2093.

[54] M.-H. Hsieh and C.-H. Wei, "Channel estimation for OFDM systems based on comb-type pilot arrangement in frequency selective fading channels," *IEEE Trans. Consum. Electron.*, vol. 44, no. 1, pp. 217–225, Feb. 1998.

[55] A. K. Jagannatham and B. D. Rao, "Whitening-rotation-based semi-blind MIMO channel estimation," *IEEE Trans. Signal Process.*, vol. 54, no. 3, pp. 861–869, Mar. 2006.

[56] N. Michelusi, "Semi-blind channel estimation for lte downlink," Master's thesis, Thechnical University of Denmark, jun 2009.

[57] M. M. Rana, J. Kim, and W.-K. Cho, "Low complexity downlink channel estimation for LTE systems," in *Advanced Communication Technology (ICACT), 2010 The 12th International Conference on*, vol. 2, Phoenix Park, 2010, pp. 1198–1202.

[58] B. Karakaya, H. Arslan, and H. A. Curpan, "Channel estimation for LTE uplink in high Doppler spread," in *Wireless Communications and Networking Conference, 2008. WCNC 2008. IEEE*, Las Vegas, NV, 2008, pp. 1126–1130.

[59] A. Ancora, C. Bona, and D. T. M. Slock, "Down-sampled impulse response least-squares channel estimation for LTE OFDMA," in *Acoustics, Speech and Signal Processing, 2007. ICASSP 2007. IEEE International Conference on*, vol. 3, Honolulu, HI, 2007, pp. 293–296.

[60] B. Hassibi, A. H. Sayed, and T. Kailath, "H optimality of the lms algorithm," *IEEE Trans. Signal Process.*, vol. 4, no. 2, pp. 267–280, Aug. 1995.

[61] J. Berkmann, C. Carbonelli, F. Dietrich, C. Drewes, and W. Xu, "On 3G LTE terminal implementation - standard, algorithms, complexities and challenges," in *Wireless Communications and Mobile Computing Conference, 2008. IWCMC '08. International*, Crete Island, 2008, pp. 970–975.

[62] "Requirements for eutra and eutran,," 3GPP, Tech. Rep., 2006.

[63] J. G. Proakis, *Digital Communications*. McGraw-Hill, 2001.

[64] M. K. Ozdemir and H. Arslan, "Channel estimation for wireless OFDM systems," *IEEE Commun. Surveys Tuts.*, vol. 9, no. 2, pp. 18–31, 2007.

[65] Z. Jianhua and Z. Ping, "An improved 2-dimensional pilot-symbols assisted channel estimation in OFDM systems," in *Vehicular Technology Conference, 2003. VTC 2003-Spring. The 57th IEEE Semiannual*, vol. 3, Jul. 2003, pp. 1595–1599.

[66] A. Dowler, A. Doufexi, and A. Nix, "Performance evaluation of channel estimation techniques for a mobile fourth generation wide area OFDM system," in *Vehicular Technology Conference, 2002. Proceedings. VTC 2002-Fall. 2002 IEEE 56th*, vol. 4, Dec. 2002, pp. 2036–2040.

[67] R. W. S. Alan V. Oppenheim, *Discrete-Time Signal Processing,*. New Jersey: Prentice-Hall Inc., 1999.

[68] J. Wang, S. Zhu, and L. Wang, "On the channel capacity of MIMO-OFDM systems," in *Communications and Information Technology, 2005. ISCIT 2005. IEEE International Symposium on*, 2005, pp. 1372–1375.

[69] H. Bölcskei, D. Gesbert, and A. J. Paulraj, "On the capacity of OFDM-based spatial multiplexing systems," *IEEE Trans. Commun.*, vol. 50, no. 2, pp. 225–234, Feb. 2002.

[70] G. Caire and H. Shirani-Mehr, "Feedback schemes for multiuser MIMO-OFDM downlink," in *Information Theory and Applications Workshop*, San Diego, CA, 2008, pp. 33–40.